JOURNAL OF GEOPHYSICAL RESEARCH, VOL. , NO. , PAGES 1–26,

A Modeling Study of an East Asian Convective Complex During March 2001

Matthew H. Hitchman, Marcus L. Buker, Ryan D. Torn, Gregory J. Tripoli

Department of Atmospheric Sciences, University of Wisconsin - Madison

R. B. Pierce, J.A. Al-Saadi

NASA Langley Research Center, Hampton VA

M. L. Buker, M. H. Hitchman, R. D. Torn, and G. J. Tripoli, Department of Atmospheric and Oceanic Sciences, University of Wisconsin-Madison, 1225 W. Dayton St., Madison, WI 53706. (e-mail: marcus@aos.wisc.edu; torn@atmos.washington.edu; matt@aos.wisc.edu; tripoli@aos.wisc.edu)

J. A. Al-Saadi, and R. B. Pierce, NASA Langley Research Center, Hampton, VA (e-mail: j.a.al-saadi@larc.nasa.gov; r.b.pierce@larc.nasa.gov)

Abstract. During March-April 2001 forecasts from the University of Wisconsin Nonhydrostatic Modeling System (UWNMS) provided information for flight planning and estimation of stratosphere/troposphere exchange (STE) of ozone over East Asia in support of the Transport and Chemical Evolution over the Pacific (TRACE-P) mission. The 55 km resolution forecast prepared for the morning of March 23 predicted the formation of a convective complex over China and eastward propagation into the Pacific. Notable features included ingestion of polluted boundary layer air over China and marine air over the Pacific, splitting of the westerly jet, gravity wave radiation, and an annulus of stratospheric ozone descending around its periphery into the mid-troposphere. A new two-scale method for quantifying ozone flux is introduced into a 30 km resolution UWNMS hindcast and compared with DC8 flight 14 ozone observations on March 24. A thin layer of ∼100 ppbv ozone encountered near 6.5 km on the outbound leg is interpreted as due to subsidence around the periphery of the convection, contrasting with ∼65 ppbv ozone in the convective outflow in the layer 8-12 km. It is estimated that $\sim 10^{29}$ ozone molecules s^{-1} entered the troposphere from the stratosphere during this convective event, comparable to STE in midlatitude cyclones. UWNMS experiments with wet removal of butanol are compared with DC8 observations of alcohols. Results suggest that some alcohol surfactants may significantly influence uptake of other species on aerosols.

1. Introduction

Two goals of the Transport and Chemical Evolution over the Pacific (TRACE-P) mission over East Asia during March and April 2001 were to quantify the contribution of stratospheric ozone to observed tropospheric ozone, and to examine how hydrometeors and chemicals interact within cloud systems [*Jacob et al.*, 2003]. East Asia is a strong source of pollutants and is a region of intense cyclogenesis and associated descent of ozone from the stratosphere [e.g., *Danielsen et al.*, 1987]. An interesting convective complex was sampled on DC8 flight 14 on March 24. The University of Wisconsin Nonhydrostatic Modeling System (UWNMS) was used to investigate stratosphere/troposphere exchange (STE) over East Asia and the transport and uptake of alcohols. A companion paper by *Kittaka et al.* [2003] addresses sulfur chemistry issues for this convective system.

Pierce et al. [2003] analyzed the ozone budget for the entire TRACE-P mission (March 7 - April 12) using the Regional Air Quality Modeling System (RAQMS) over a 6600 x 4500 km domain at a 110 km resolution, with on-line chemical calculations. They found that tropospheric production exceeded STE by a factor of 7, but was largely offset by dry deposition. They used the formalism of *Wirth and Egger* [1999] to calculate the cross-tropopause ozone flux per unit horizontal area:

$$F_{WE} = \frac{\chi_{O_3}(\vec{V} - \vec{C}_{tpp}) \cdot \hat{n}}{cos\alpha}, \tag{1}$$

where χ_{O_3} is ozone number density, $\vec{V}$ is the 3D wind at the tropopause, $\vec{C}_{tpp}$ is the 3D motion of the tropopause, $\hat{n}$ is the normal to the tropopause, and α is the angle between $\hat{n}$ and the zenith. *Pierce et al.* [2003] used a temperature lapse rate definition of the tropopause, which is essential for representing both the tropical and extratropical tropopause structures in their large domain. If vertical motions vary with altitude, adia-

batic temperature changes can lead to the location of the tropopausal lapse rate threshold value moving relative to a material surface. In the present analysis the UWNMS, the regional component of RAQMS, is used to examine an alternative approach to estimating STE, where the tropopause is defined by potential vorticity (PV) surfaces.

1.1. The two-scale method

For adiabatic inviscid flow the tropopause defined by potential vorticity or potential temperature is a material surface, hence $\vec{V} = \vec{C}_{tpp}$ and $F = 0$ [e.g., *Haynes and McIntyre*, 1990]. For a conserved constituent, motion of the tropopause relative to constituent isopleths can occur only if there is non-zero heating or irreversible mixing. Non-zero F for the $\partial T/\partial z$-defined tropopause in the RAQMS can occur whenever the tropopause moves relative to resolved wind motions, due to differential adiabatic vertical motions, grid-resolved diabatic heating, and parameterized subgrid-scale diffusion. Non-zero F for the UWNMS PV tropopause can only occur through resolved diabatic heating and subgrid-scale diffusion.

Observational and theoretical work shows that filamentous intrusion into the troposphere occurs by differential advection and deformation on a wide range of scales [e.g., *Shapiro*, 1980; *Hoskins et al.*, 1985; *Danielsen et al.*, 1987; *Reid and Vaughn*, 1991; *Holton et al.*, 1995; *Haynes and Anglade*, 1997; *Sato and Dunkerton*, 2002]. Thus, sub-grid scale diffusive parameterizations are a crude proxy for actual cross-tropopause flux. Furthermore, photon exchange and radiative damping of rapidly-evolving adjacent thermal perturbations increases quickly with reduced scale [*Haynes and Ward*, 1993] and is much larger than climatological net heating rates near the tropopause, which are typically less than 0.5 K/day [e.g., *Kiehl and Solomon*, 1986; *Shine*, 1987]. These factors motivated us

to postulate a new two-scale method, where flux across a smoothed, large-scale surface is the result of motions at smaller scales. It makes use of explicitly resolved motions in a synoptic-mesoscale model and assumes that mixing processes inevitably cascade to the Kolmogorov microscale.

Buker et al. [2003] explores the dependence of ozone flux on model resolution and degree of smoothing in the two-scale method and applies it in the UWNMS to the case of March 26, 2001 (DC8 flight 15), which was characterized by a strongly filamented jet and developing cyclone. Fundamental assumptions in the two-scale method include a) filamentous intrusions at sub-synoptic scales are irreversibly mixed, b) the synoptic scale tropopause is continuously restored by viscous, diabatic processes. In the case of the tropopause, it is defined and advected by smoothed wind fields, with higher-resolution winds determining the cross-tropopause flux. This provides an upper bound on STE under the assumption of complete irreversible mixing of air that crosses the smoothed tropopause. By varying the degree of smoothing one may evaluate the relative contributions to STE by a range of model-resolved scales. The two-scale method attempts to directly assess the combined effects of phenomena at scales below the smoothing scale, such as ageostrophic motions associated with synoptic scale flows, inertia-gravity waves, layered structures due to inertial instability [*Sato and Dunkerton*, 2002], the 2D and 3D enstrophy cascade, and chaotic mixing. The two-scale method is quite general and allows for quantification of fluxes across other surfaces of interest, not just that corresponding to the tropopause. Calculation of flux convergences provides the transport component for the budget of a chosen constituent.

In this paper we highlight the importance of convective complexes for STE and apply our new two-scale method relative to potential vorticity (PV) surfaces to quantify ozone transport for the event of March 24. In this application, winds are smoothed with a bi-directional 1-2-1 filter applied m times on modeled constant altitude surfaces to yield a response function at scale L given by

$$R_m = cos^{2m}\left(\frac{\pi\delta x}{L}\right), \tag{2}$$

where δx is the horizontal resolution of the model. The motion of the smoothed PV surface is given by $\vec{V_s}\cdot\hat{n}$, where $\vec{V_s}$ is the smoothed wind field and $\hat{n} = \vec{\nabla}P_s/|\vec{\nabla}P_s|$ is the normal to the smoothed PV surface. Retaining the full model-resolved motion field as $\vec{V}$, the flux of ozone across a smoothed PV surface of arbitrary orientation is

$$F_{2-scale} = \chi_{O_3}(\vec{V} - \vec{V_s})\cdot\hat{n}. \tag{3}$$

1.2. Alcohol surfactants

Surfactants can reduce the ability of gas molecules to penetrate into the bulk of both water and sulfuric acid droplets by forming a monolayer surface at low solute concentrations [*La Mer*, 1962; *Porter et al.*, 1996; *Ellison et al.*, 1999]. These surfactants are not just limited to long-chain, man-made compounds, but include simpler natural organic alcohols [*Singh et al.*, 1995; *Murphy et al.*, 1998]. Alcohols are common in the planetary boundary layer, with emissions from both agricultural and industrial processes [*Cavanagh et al.*, 1969; *Snyder and Dawson*, 1985; *Konig et al.*, 1995]. Higher ethanol concentrations have been found in urban areas where ethanol-based gasolines are used in transportation [*Grosjean*, 1997].

Torn et al. [2002] carried out a combination of laboratory work and experiments with the UWNMS to explore the possiblity that butanol may significantly interfere with the uptake of other species on aerosols in the upper troposphere and lower stratosphere (UTLS). Using surface tension measurements at 294 K, the surface concentration of butanol decreased from 3.5 x 10^{14} cm^{-2} for pure water to 2.0 x 10^{14} cm^{-2} for 72% sulfuric acid by weight. Substitution of hexanol for butanol or decreasing the temperature to 208 K doubled the surface concentration. Longer-chain alcohols saturate the surface more readily than ethanol and methanol. These measurements provided a minimum atmospheric concentration necessary to create near-monolayer coverage of a sulfuric acid aerosol. For an aerosol concentration of 5 μm cm^{-3}, using the minimum butanol concentration of 2 x 10^{-16} mol cm^{-3} to create a monolayer, an atmospheric butanol concentration of $\sim$1.0 ppbm would be required to create a saturated surface. UWNMS experiments with parameterized wet removal of butanol were carried out and compared with DC8 alcohol data.

Section 2 gives a brief description of previous work with the UWNMS, forecasts made for TRACE-P, and and observations used in this study. The UWNMS forecast for March 24, 2001 is described in section 3, where a convective complex was anticipated to form over China and propagate eastward over the Pacific south of Japan. A higher-resolution hindcast of this event is compared in detail with aircraft observations in section 4, with a focus on using our new two-scale method for calculating ozone transport near the convection. In section 5 TRACE-P measurements of alcohols are compared with UWNMS experiments on butanol for this convective case study. A summary is given in section 6.

2. UWNMS and Observations

2.1. Previous work with the UWNMS

The UWNMS was initially designed to study tropospheric scale interaction problems and has been applied to tropical cloud clusters, hurricanes, midlatitude cyclones, polar lows, gravity waves, lake effect snow storms, and mesoscale convective complexes [*Tripoli*, 1992a, b; *Pokrandt et al.*, 1996; *Mecikalski and Tripoli*, 1997; *Avissar et al.*, 1998]. It includes multiple interactive grid nesting, tropospheric microphysics, radiative transfer, surface processes, and 1/6° (∼18.5 km) resolution topography. Operational tropospheric weather forecasts are available daily on the internet at *http://mocha.aos.wisc.edu*.

The UWNMS has been adapted for application to transport problems involving the troposphere and lower stratosphere. *Hitchman et al.*, [1999] showed that downward ozone transport by synoptic waves out of the arctic summer stratosphere contributed significantly to the observed decline of column ozone during the Polar Ozone Loss in Arctic Regions in the Summer (POLARIS) campaign. During the Sage III Ozone Loss and Validation Experiment (SOLVE) of December 1999 - March 2000 a variety of polar stratospheric clouds (PSCs) were detected. The UWNMS was used in the field for flight guidance and diagnosis of the dynamical causes of the PSCs. It was found that many of the PSCs, particularly in December 1999, were not linked to flow over orography, but were due to inertia-gravity waves radiating into the cold pool from the adjusting polar front jet at the tropopause [*Hitchman et al.*, 2003]. The meso-synoptic scale UWNMS has been combined with a global isentropic model [*Johnson et al.*, 1993] and a detailed chemistry package from the Langley IMPACT model [*Eckman et al.*, 1995] to create the RAQMS [*Pierce et al.*, 2003].

2.2. Overview of UWNMS forecasts for TRACE-P

The TRACE-P campaign included instrumented flights from Hong Kong and Yokota, Japan during March and April 2001 [*Jacob et al.*, 2003]. For each of the DC8 and P3 flights a forecast by the UWNMS was made available for discussion by the TRACE-P science team by 10 am the day before the flight. These simulations were initialized with 1°x 1° resolution aviation model (AVN) forecasts from the National Centers for Environmental Prediction, together with PV-mapped ozone fields derived with the method of *Pierce et al.* [1999]. Each simulation was started 60 hours prior to the end of the scheduled flight and integrated with 55 km horizontal and 400 m vertical resolution at a time step of 60 s. The center of the domain was located at 130°W, 30°N, with a grid of 90 x 90 points in the horizontal and 55 in the vertical. Convective parameterizations were turned off; vertical motions were calculated explicitly. The horizontal boundaries of the UWNMS were updated every time step from a temporal and spatial interpolation of the 6-hourly 1.0° AVN forecast files. An 8-point Rayleigh friction sponge layer was applied approaching the top of the domain at 22 km altitude. A 5-point Rayleigh friction zone at the horizontal boundaries was implemented to suppress spurious wave reflection.

Model variables were archived every 5 minutes for diagnosis using VIS-5D [*Hibbard et al.*, 1989]. An idealized tracer, initialized to decrease linearly at all locations from 1 at the surface to zero at 22 km, was useful for visualizing transport associated with convection and synoptic scale flows. The idealized tracer and ozone were treated as conserved quantities. VIS5D output included 3D winds, pressure, temperature, potential temperature, potential vorticity, perturbation equivalent potential temperature, water vapor mixing ratio, precipitable water content, idealized tracer, and ozone.

2.3. TRACE-P validation data sets

Images from infrared, visible, and water vapor channels on Japan's Geostationary Meteorology Satellite 5 (GMS-5), as well as meteorological analyses and back trajectories created by TRACE-P science team members, were obtained during the campaign. Time-altitude sections of Langley DIAL ozone [*Browell et al.*, 2003] and in situ ozone at flight level allow comparison with UWNMS ozone features. In situ measurements of methanol, ethanol, and butanol [*Apel*, 2003; *Singh et al.*, 1995], provide useful constraints on interpretating UWNMS experiments with butanol.

3. UWNMS forecast for DC8 Flight 14 on March 24

The 55 km resolution UWNMS forecast for March 24, available at 10 am March 23, departed from the 111 km AVN forecast in that it clearly showed the development of a convective complex northeast of China and subsequent propagation eastward into a region observable by the DC8. The forecast was initialized at 0600 UT (2 pm local time) March 21 and integrated for 84 hours, through 1800 UT March 24 (3 am March 25 local time). At the flight planning meeting it was argued that this would be an excellent opportunity to address one of the goals of TRACE-P, to evaluate how deep convection redistributes and modifies polluted continental and cleaner marine air transported from the boundary layer. By 4 pm local time March 23 GMS satellite imagery confirmed the convective development and the decision was made to combine the goal of sampling the convection with the original goal for flight 14, to make correlative measurement of carbon monoxide in cloud-free air for a Measurements of Pollution in the Troposphere (MOPITT) satellite instrument overpass [*see Kiley et al.*, 2003]. One of the authors (MHH) was on this flight,

which lasted from 2310 UT March 23 to 0820 UT March 24 (8:10 am - 5:20 pm local time).

Figure 1 shows GMS-5 enhanced infrared images for a sequence of times during the convective event. At 0631 UT March 23 (3:31 local time) the convective complex was near 30°N, 115°E, appearing as a blue area approximately 400 km x 400 km in Figure 1a, with cloud top temperatures near -50°C. The upper tropospheric water vapor image (not shown) revealed enhanced amounts, indicative of water vapor injection from the boundary layer into the upper troposphere and downstream of the convection.

Figures 2-4 show the UWNMS forecast presented at the flight planning meeting on March 23, including anticipated effects of the convection on the distribution of water vapor, idealized tracer, jet maximum, and ozone. At 2200 UT March 23 (7 am March 24 local) the sea level pressure distribution showed a weak high centered over central Japan, with a northeast-southwest oriented band of low pressure over northeast China (Fig. 2). A low pressure center near the east coast of China coincided with the region of convection seen in the infrared satellite image in Figure 1a. Moist boundary layer air from southern China (orange) was predicted to ascend along the 300 K surface northeastward into the convective region (Fig. 2).

Figure 3 shows an east-west section through the convective region and the sea level pressure distribution (white contours) at 0300 UT March 24 (noon local time). The surface low was forecast to be located slightly offshore, with upward motions exceeding 0.1 m/s (pink) at its eastern edge. The idealized tracer initialized to be 1 at the surface (orange) and 0 at the top (purple) suggested the ventilation of moist, polluted boundary layer air into the upper troposphere, with detrainment out its eastern edge near the tropopause.

Note the signature of descending stratospheric air (blue) around the periphery of the convection. UWNMS ozone values of ∼100 ppbv were forecast near the tip of the blue region at 6 km to the east of the convection (not shown). Based on this forecast it was anticipated that a spiral ascent into the convective outflow might yield a chemical signature of interaction with hydrometeors, [e.g., *Cohan et al.*, 1999].

Potential temperature contours (black) in Figure 3 suggested that the tropopause near 340 K would be deformed upward over the convection. Above the convective updraft, coherent undulations may be seen in the potential temperature contours tilting westward with height, indicating upward and westward propagation of gravity wave energy away from the convective source. Individual wave crests moved westward and downward with time relative to the convection (not shown). Horizontal and vertical wavelengths are estimated to be ∼1000 km x ∼10 km, giving a westward intrinsic trace speed of ∼30 m/s. Such waves tend to break due to Kelvin-Helmholz instability, leading to mixing in the lowest stratosphere [e.g., *Sato*, 1994; *Alexander and Pfister*, 1995].

A horizontal slice at 12.5 km in the UWNMS forecast for 0400 UT (1 pm local time) March 24 predicted that the convective complex would penetrate vertically through the subtropical westerly jet (Figure 4). The 53 m/s isosurface is shown in light purple, indicating that some of the strong westerly flow is deflected northward around the complex. The rapid eastward progression of the convection is due to being imbedded in this westerly jet. The model PV contours (black) also anticipated that a portion of tropical upper tropospheric air would curve out of the jet clockwise around the convection, while low momentum air ascended from the boundary layer to the jet level and was detrained above 10 km. This may be interpreted as a roughly cylindrical convective updraft which created

a form drag on the jet. This represents a substantial westward torque on the subtropical westerly jet, an extratropical example of "cumulus friction" [*Schneider and Lindzen*, 1976].

4. Flight 14 observations

Figures 1b-d depict the east-southeastward progression and weakening of the convective complex over the Pacific. It reached the coast of China by 1231 UT (9:31 pm local) on March 23 (Figure 1b). About an hour after the DC8 took off the next morning the convective system was still strong and centered south of Japan (0031 UT, 9:31 am local time on March 24; Figure 1c). Six hours later when the aircraft flew through the system it had weakened and spread out (0631 UT, 3:31 pm local time on March 24; Figure 1d). Approaching the system one could see multiple layers of diffuse clouds without any distinct visual center to the system.

Figure 5 shows the flight track superimposed on a GMS-5 infrared image at 0332 UT (12:32 pm local time). A thin layer of high ozone was seen near 6.5 km altitude on the ozone sensor readout during the ascent at ∼0040 UT (9:40 am local), possibly indicative of a stratospheric intrusion. Near 0205 UT (11:05 am local) no cirrus was observed overhead as the plane circled downward, taking a carbon monoxide profile for comparison with the MOPITT overpass. At ∼0430 UT (1:30 pm local) the DC8 entered a stratocumulus deck at 1200 m. By 0520 (2:20 pm local) clouds were seen overhead at ∼4-6 km. Near 0545 UT (2:45 pm local) lightning was detected 150 km to the east, indicating a cluster of thunderstorms that were still active, embedded within the broader cloud mass. At 0617 UT (3:17 pm local) the aircraft began a spiral ascent through air with relatively low amounts of ozone. At ∼0645 UT (3:45 pm local) the message came over the headphones

that further ascent was not allowed due to an aircraft overhead. Thus, ascent within the clouds was curtailed near 24,000'. Ascent resumed farther north to 33,000' by 0720 UT (4:20 pm local), with cirrus clouds observed overhead near 12 km.

The Langley DIAL ozone data for this flight are shown in Figure 6. Values less than 40 ppbv were seen in the marine boundary layer. Values exceeding 100 ppbv were seen above 12 km during the first two hours and last hour of the flight, corresponding to times when the aircraft was farthest north, detecting extratropical stratospheric ozone. During the first two hours ozone amounts exceeding 80 ppbv were seen near 6 km, with a layer of ozone-poor air between 7 and 10 km. UWNMS results suggest that this structure resulted directly from the convective transport of high ozone down to 6 km around its periphery, with detrained low ozone centered near 9 km. Due to the presence of clouds the DIAL did not sense the upper troposphere during 0430-0630 UT.

DC8 flight altitude and in situ ozone mixing ratio are shown as a function of time in Figure 7. Near 0200 UT and 0330-0430 UT the aircraft was at or above 8 km, with ozone values exceeding 70 ppbv. Near 0040 UT at 6.5 km a spike of 100 ppbv ozone was observed. During 0630-0730 UT ozone decreased below 70 ppbv within the convective complex and its outflow in the layer 8-10 km.

Ozone mixing ratio is presented as a function of altitude in Figure 8 for six flight segments during which substantial ascent or descent occurred. The locations may be inferred from the times labelled on Figure 5. These include a) ascent from Yokota, b) descent near 28°N, 150°E, c) ascent near 26°N, 150°E for the MOPITT underpass, d) descent near 22°N, 142°E, e) ascent in the convective complex near 28°N, 136°E, and f) descent into Yokota. Panel a) shows a layer layer of enhanced ozone near 6.5 km during

the ascent from Yokota, peaking at 100 ppbv, with a vertical half-width for the anomaly of ∼500 m. Panels b), c), and d) show ozone exceeding 80 ppbv descending from ∼9 to 8 km. Panel e) shows less than 70 ppbv ozone close to the convective complex above 9 km. For the time shown in panel e, the temperature and dew point (not shown) were equal to each other from 500 m to 6500 m, confirming that the aircraft was within the clouds. Another narrow spike of high ozone was seen near 5 km in panel f) on descent to Yokota. The ozone spikes in panels a) and f) coincided with layers of anomalously low dew point (not shown). These observations are interpreted in the context of a higher resolution UWNMS simulation in the next section.

5. 30 km resolution UWNMS hindcast with ozone flux calculation

5.1. UWNMS hindcast for March 24

The two-scale method for evaluating the flux of material across PV surfaces was developed after the TRACE-P mission. To more accurately diagnose the case of March 24 a UWNMS hindcast was made at 30 km resolution. The period of integration and domain size (5000 x 5000 km) was the same as for the forecast described in section 3. A more refined data set for ozone initialization was obtained from the TRACE-P mission RAQMS simulation. Cross-tropopause ozone flux was calculated with the two-scale method for a range of applications of the bi-directional 1-2-1 filter. Results are shown for $m = 42$ in equation 2, with R(400 km) = 0.095 and R(1000 km) = 0.69. Thus the convective complex is regarded as part of the motions which contribute to STE.

Figure 9 shows the horizontal distribution of ozone at 6.5 km and a vertical section along the flight track at 0100 UT (10 am local time). Values less than 50 ppbv are seen in the model over the southeastern tip of Japan, with a values near 100 ppbv near the

flight track. The vertical section shows that the DC8 flew through a downwelling plume of stratospheric air which curved westward toward the convective center near 6.5 km, reminiscent of a wide variety of numerical simulations and observations of the circulation near a warm bubble. The modeled region of 40-50 ppbv ozone in the layer 8-12 km agrees in location and value with the layer of reduced ozone in the DIAL observations (compare Figs. 10b and 6). Note also the westward-tilting inertia-gravity waves in the ozone pattern in the stratosphere downstream of the convection, suggestive of strong disturbances ahead of the rapidly moving convective tops and imminent mixing of air in UTLS.

Figure 10 shows the horizontal distribution of ozone at 9 km and a vertical section along the flight track at 0700 UT (4 pm local time). The region of 40-50 ppbv ozone in the 8-12 km layer above the flight track has moved eastward, with values near 65 ppbv at flight location (cf. Fig. 9d). At this time the aircraft was sampling higher ozone from the intrusion curling in from the west around the convective plume. The vertical section further illustrates the evolving downward plumes of high ozone around the updraft of ozone-poor air in this aging convection.

UWNMS 10 km streamlines (white arrows), near-tropopause PV values (black contours), and shaded values of ozone flux for 0100 UT (10 am local time) are shown in Figure 11. Note the poleward redirection of the westerly jet around the convection region. The tropopause depicted in PV contours is also deformed poleward in this region, with filaments of high PV found to the south, east, and west of the convection. The radius of the disturbed region exceeds 1000 km. White regions indicate downward ozone flux, which occurs near the west, southeast, and northeast edges of the convection.

Figure 12 shows a longitude-altitude section of UWNMS streamfunction in the plane, PV contours (black) and ozone flux (shaded) at 1 pm on March 24. High values of PV are seen on the periphery of the convection and also in the lower portions of the convection. The latter is due to latent heating maximizing in the mid-troposphere, increasing the static stability, hence PV, in the lower troposphere. The streamlines show the rapid ascent of boundary layer air and detrainment at upper levels. Downward extension of stratospheric air is seen around the periphery, coinciding with a flux of ozone into the troposphere. The stratospheric intrusion to the east of the convection is located farther away from the convective center due to the detrainment of tropospheric air into the westerly jet.

Figure 13 shows the history of net ozone flux across the 1.3 potential vorticity unit surface (PVU; 10^{-6} m^2 K kg^{-1} s^{-1}), integrated over the model domain for the entire simulation. An initial model dynamical adjustment is seen during the first hour, then the ozone flux varies around -1x10^{28} ozone molecules s^{-1} for the first 36 hours. From 1200 UT March 23 - 0000 UT March 24 the flux averaged -5x10^{28} ozone molecules s^{-1}. On March 24 the ozone flux averaged -8x10^{28} ozone molecules s^{-1}.

An idealized calculation may be made for comparison. Assume that an annulus of 100 ppbv ozone with inner and outer radii 1000 and 1500 km, extending from 5 to 10 km altitude is irreversibly mixed into the troposphere over a 24 hour period. Then $\sim$10^{29} ozone molecules s^{-1} will enter the troposphere over this 5000 x 5000 km domain, similar in magnitude to results from the two-scale method. This corresponds to $\sim$5x10^{11} ozone molecules cm^{-2} s^{-1}, which is similar in magnitude to the results of *Pierce et al.* [2003]. This is comparable to the downward averaged flux across 7 km over East Asia reported by

Carmichael et al. [1998] during early May 1987. Convective systems such as the present case can cause STE comparable to strong cyclogenesis.

6. Alcohol Observations and UWNMS experiments

The time variation of methanol, ethanol, and butanol are shown in Figure 14. There is a general correlation between higher alcohol amounts and altitude, with values of 2-4 ppbv methanol and 100-250 pptv ethanol in the 5-10 km altitude range. In contrast, butanol maximized in the boundary layer, reaching 200-300 pptv. In the convection and outflow during ∼0630-0745 UT, high levels of methanol and ethanol were found, but butanol was about 50 pptv (about 25% of surface values).

For experiments with the UWNMS two removal mechanisms were considered. OH radicals react with the CH_2 groups on the alcohol chain, removing one of the hydrogens to produce water. Longer-chain alcohols and greater OH concentration lead to faster reduction of alcohol concentration. The half-life of methanol and ethanol is five times that of butanol. The elevated amounts of methanol and ethanol relative to butanol at 5-10 km altitudes are consistent with upstream surface sources several days before. For the convective case of March 24 OH concentrations were small enough that dry removal can be ignored relative to wet removal for butanol. A global wet deposition flux for butanol may be estimated by assuming a seasonal precipitation of 30 cm, a Henry's Law constant of 26 x 10^3 M atm^{-1} at 273 K [*Snyder and Dawson*, 1985] and a mean butanol concentration of 500 pptv. By dividing the column total butanol concentration by the butanol flux, one gets 100 days as a characteristic removal time of all butanol by wet deposition. This is scaled by the local rainfall rate calculated in the UWNMS for parameterized wet loss in the model.

The UWNMS was run in the same configuration as the forecast described in section 3 for the outer grid, with an inner grid of 60 x 60 points at 18 km resolution. The 400 m and 800 m layers were initialized with a concentration of 5 ppbm butanol. A run with no removal processes is compared with a run with only wet removal in Figure 15. In the conserved case maximum butanol mixing ratios at 10 km in and near the convection were ∼2.5 ppbm, diluted by mixing to about half of the initialized boundary layer value. Inclusion of parameterized wet removal reduces butanol at 10 km to less than 1.2 ppbm. Approximately half of the butanol reaching the upper troposphere in the conservative case is removed by passage through the cloud. In the wet removal case detrained butanol in the upper troposphere is about 25% that of the boundary layer values, consistent with the observations.

Close to heavily polluted areas with ∼5 ppbm in the boundary layer, convective transport can inject ∼1 ppbm (∼300 pptv) into the lower stratosphere, enough to saturate a sulfuric acid aerosol concentration of 5 μm cm^{-3}. DC8 observations show that butanol concentrations were about 1/10 of that amount in the upper troposphere. But concentrations of other alcohols were much higher. This study suggests that butanol and other alcohols are of the right order of magnitude for significantly affecting aerosol uptake and heterogeneous reactions for other species in the UTLS.

7. Conclusions

Aircraft sampling of the convective event on March 24, 2001 provided a unique opportunity to study how it affected the distribution of climatologically important trace gases. It highlights the utility of having mesoscale resolution forecasts available in the field and flexibility for flight decisions. Even at 55 km resolution many mesoscale convective com-

plexes can be represented reasonably well in nonhydrostatic models that calculate vertical motions explicitly. Ozone fields from the RAQMS used to initialize the UWNMS provided a good representation of synoptic-scale ozone structure, while the 30 km UWNMS run evolved more mesoscale ozone features, including downwelling around the periphery of the convective complex. A detailed comparison of aircraft with the 30 km resolution UWNMS simulation verified the primary new result of this work: significant amounts of ozone can enter the troposphere on the periphery of extratropical convection that reaches the stratosphere. Specific features in the simulation agreed well with observations, including the 6.5 km 100 ppbv ozone filament from the stratosphere and the vault of lower ozone detrained from the convection at 8-12 km altitude.

The new two-scale method was applied to this convective situation with good success. It has the advantages of making use of resolved motions in the model and addresses the issue that adiabatic inviscid motion cannot transport material across the tropopause. Ozone STE was markedly enhanced during the lifetime of the convective event, with $\sim 10^{29}$ molecules s^{-1} entering the troposphere. The convection deforms the ozone pattern in the lowest stratosphere, coinciding with inertia-gravity waves radiating away from the convection. It is of interest to pursue this component of STE in the future. The role of convection in eroding the tropopause upward during summertime [e.g., *Langford et al.*, 1996] is not widely appreciated. The present work suggests that STE associated with deep convection is quantitatively important with respect to the global budgets of ozone and other climatologically important trace species. Initial studies with butanol suggest that convective transport of alcohols may yield significant surfactant concentration in the

UTLS to modify heterogeneous chemistry on aerosol. These avenues of research will be pursued in future modeling work with the UWNMS.

Acknowledgments. We thank the TRACE-P science team for their careful measurements, planning, and analysis which made this work possible. We gratefully acknowledge support from NASA TRACE-P Grant NCC1-01-011 and ACMAP Grant NAG5-11303.

References

Alexander, M. and L. Pfister, Gravity wave momentum flux in the lower stratosphere over convection. *Geophys. Res. Lett.*, **22**, 2029-2032.

Apel, E., A. Hills, R. Lueb, S. Zindel, S. Eisele, D. Reimer, A fast-GC/MS system to measure C2 to C5 carbonyls, methanol, and ethanol aboard aircraft, *J. Geophys. Res., in press*, 2003.

Avissar, R., E. Eloranta, K. Gurer, and G. J. Tripoli, An evaluation of the large eddy simulation option of the Regional Atmospheric Modeling System in simulating the convective boundary layer: A Fife case study, *J. Atmos. Sci.*, *55*, 1109-1130, 1998.

Browell, E. V., et al., Large-scale ozone and aerosol distributions, air mass characteristics, and ozone fluxes over the western Pacific Ocean in the late winter/early spring. *J. Geophys. Res., in press*, 2003.

Buker, M. L., M. H. Hitchman, and R. B. Pierce, Resolution dependence of cross-tropopause ozone transport over East Asia. *Submitted to J. Geophys. Res.*, 2003.

Cavanagh, L. A., C. F. Schadt, F. Conrad, and E. Robinson, *Environ. Scie. Technol.*, **3**, 251, 1969.

Carmichael, G. R., I. Uno, M. J. Phadnis, Y. Zhang, and Y. Sunwoo, Tropospheric ozone production and transport in the springtime in east Asia, *J. Geophys. Res.*, **103**, 10,649-10,671, 1998.

Cohan, D. S., M. G. Schultz, D. J. Jacob, B. G. Heikes, and D. R. Blake, Convective injection and photochemical decay of peroxides in the tropical upper troposphere: Methyl iodide as a tracer of marine convection, *J. Geophys. Res.*, **104**, 5717-5724, 20 March 1999.

Danielsen, E. F., R. S. Hipskind, S. E. Gaines, G. W. Sachse, G. L. Gregory, and G. F. Hill, Three-dimensional analysis of potential vorticity associated with tropopause folds and observed variations of ozone and carbon monoxide, *J. Geophys. Res.*, **92**, 2103-2111, 1987.

Eckman, R. S., W. L. Grose, R. E. Turner, W. T. Blackshear, J. M. Russell III, L. Froidevaux, J. W. Waters, J. B. Kumer, and A. E. Roche, Stratospheric trace constituents simulated by a three-dimensional general circulation model: Comparison with UARS data, *J. Geophys. Res.*, **100**, 13,951-13,966, 1995.

Ellison, G. B., Tuck, A. F., Vaida V. J., Atmospheric processing of organic aerosols. *J. Geophys. Res. Atmos.*, **104**, 11,633-11,641, 1999.

Grosjean, D., *J. Braz. Chem. Soc.*, **8**, 433, 1997.

Haynes, P. H., and M. E. McIntyre, On the conservation and impermeability theorems for potential vorticity. *J. Atmos. Sci.*, **47**, 2021-2031, 1990.

Haynes, P. H., and W. E. Ward, The effect of realistic radiative transfer on potential vorticity structures, including the influence of background shear and strain. *J. Atmos. Sci.*, **50**, 3431-3453, 1993.

Haynes, P., and J. Anglade, The vertical-scale cascade in atmospheric tracers due to large-scale differential advection. *J. Atmos. Sci.*, **54**, 1121-1136, 1997.

Hibbard, W. L., and D. Santek, The VIS-5D system for easy interactive visualization, in *Proceedings of Visualization '90*, pp. 28-35, IEEE Comput. Soc. Press, Los Alamitos, Calif., 1989.

Hitchman, M. H., M. L. Buker, and G. J. Tripoli, Influence of synoptic waves on column ozone during Arctic summer 1997, *J. Geophys. Res.*, **104**, 26,547-26,563, 1999.

Hitchman, M. H., M. L. Buker, G. J. Tripoli, E. V. Browell, W. B. Grant, T. J. McGee, and J. F. Burris, Non-orographic generation of arctic PSCs during December 1999. *J. Geophys. Res.*, **108**, SOL 68, 1-16, 2003.

Holton, J. R., P. H. Haynes, M. E. McIntyre, A. R. Douglass, R. B. Rood, and L. Pfister, Stratosphere-troposphere exchange, *Rev. Geophys.*, **33**, 403-439, 1995.

Hoskins, B. J., M. E. McIntyre, and A. W. Robertson, On the use and significance of isentropic potential vorticity maps. *Q. J. Roy. Meteorol. Soc.*, **111**, 877-946, 1985.

Jacob, D., J. Crawford, M. Kleb, V. Connors, R. Bendura, and J. Raper, The Transport and Chemical Evolution over the Pacific (TRACE-P) mission: Design, execution, and overview of first results, *J. Geophys. Res., in press*, 8781, 2003.

Johnson, D. R., T. H. Zapotocny, F. M. Reames, B. J. Wolf, and R. B. Pierce, A comparison of simulated precipitation by hybrid isentropic sigma and sigma models. *Mon. Weather Rev.*, **121**, 2088-2114, 1993.

Kiehl, J. T., and S. Solomon, On the radiative balance of the stratosphere. *J. Atmos. Sci.*, **43**, 1525-1534.

Kiley, C., et al., An intercomparison and evaluation of aircraft-derived and simulated CO from seven chemical transport models during the TRACE-P experiment, *J. Geophys. Res.*, **108(D21)**, 8819, in press, 2003.

Kittaka, C., et al., Effects of clouds on sulfate distribution using a three dimensional model (RAQMS), *Submitted to J. Geophys. Res.*, **108**, 2003.

Konig, G., M. Brunda, H. Puxbaum, C. N. Hewit, S. C. Duckham, and J. Rudolph, *Atmos. Environ.*. **29**, 861, 1995.

La Mer, V. K., *Retardation of Evaporation by Monolayers: Transport Processes*, Academic Press, New York, 1962.

Langford, A. O., T. J. O'Leary, M. H. Proffitt, and M. H. Hitchman, 1994: Transport of the Pinatubo Volcanic Aerosol to a Northern Midlatitude Site. *J. Geophys. Res.*, **100**, 9007-9016.

Mecikalski, J. R., and G. J. Tripoli, Inertial available kinetic energy and the dynamics of tropical plume formation, *Mon. Weather Rev.*, *126*, 2200-2216, 1997.

Murphy, D. M., D. S. Thomson, T. M. J. Mahoney, In situ measurements of organics, meteoritic material, mercury, and other elements in aerosols at 5 to 19 kilometers. *Science*, **282**, 1664-1669, 1998.

Pierce, R. B., J. A. Al-Saadi, T. D. Fairlie, J. R. Olson, R. S. Eckman, W. L. Grose, G. S. Lingenfelser, and J. M. Russell III, Large-scale stratospheric ozone photochemistry and transport during the POLARIS campaign, *J. Geophys. Res.*, **104**, 26,525-26,545, 1999.

Pierce, R. B., et al., Regional air quality modeling system (RAQMS) predictions of the tropospheric ozone budget over East Asia, *J. Geophys. Res.*, **108**, 8825, 2003.

Pokrandt, P. J., G. J. Tripoli, and D. D. Houghton, Processes leading to the formation of mesoscale waves in the midwest cyclone of 15 December 1987, *Mon. Weather Rev.*, **124**, 2726-2752, 1996.

Porter, J. J., J. K. Klassen, and G. M. Nathanson, *Langmuir*, **12**, 5448-, 1996.

Reid, S. J., and G. vaughan, Lamination in ozone profiles in the lower stratosphere. *Quart. J. Royal Meteor. Soc.*, **117**, 825-844, 1991.

Sato, K., A statistical sudy of the structure, saturation, and sources of inertio-gravity waves in the lower stratosphere observed with the MU radar. *J. Atmos. Terr. Phys.*, **56**, 755-774, 1994.

Sato, K., and T. J. Dunkerton, Layered structure associated with low potential vorticity near the tropopause seen in high-resolution radiosondes over Japan, *J. Atmos. Sci.*, **59**, 2782-2800, 2002.

Schneider, E. K., and R. S. Lindzen, A discussion of the parameterization of momentum exchange by cumulus convection. *J. Geophys. Res.*, **81**, 3158-3160.

Shapiro, M. A., Turbulent mixing within tropopause folds as a mechanism for the exchange of chemical constituents between the stratosphere and troposphere. *J. Atmos. Sci.*, **37**, 994-1004, 1980.

Shine, K. P., The middle atmosphere in the absence of dynamical heat fluxes. *Quart. J. Royal Meteor. Soc.*, **113**, 603-633, 1987.

Singh, H. B., M. Kanakidou, P. J. Crutzen, and D. J. Jacob, High concentrations and photochemical fate of oxygenated hydrocarbons in the global troposphere, *Nature*, **378**, 50-54, 1995.

Snyder, R. R., and G. A. Dawson, *J. Geophys. Res.*, **90D**, 3797, 1985.

Torn, R. D., G. M. Nathanson, Surface tensions and surface segregation of n-butanol in sulfuric acid. *J. Phys. Chem B*, **106**, 8064-8069, 2002.

Tripoli, G. J., An explicit three-dimensional nonhydrostatic numerical simulation of a tropical cyclone, *Meteorol. Atmos. Phys.*, **49**, 229-254, 1992a.

Tripoli, G. J., A nonhydrostatic numerical model designed to simulate scale interaction. *Mon. Weather Rev.*, **120**, 1342-1359, 1992b.

Figure 1. Infrared image from the GMS-5 satellite at a) 0631 UT March 23, 2001, b) 1231 UT March 23, 2001, c) 0031 UT March 24, 2001, d) 0631 UT March 24, 2001. Cloud top temperatures of ∼-50°C are associated with the convective complex which propagated eastward from eastern China to southeast of Japan.

Figure 2. UWNMS forecast for 2200 UT March 23, 2001 (7 am March 24 local time), showing sea level pressure (contour interval 4 hPa) and water vapor mixing ratio on the 300 K potential temperature surface (g/kg, color bar). Note the warm upglide ahead of the surface low from southeastern China (g/kg, color bar). High water vapor values, indicative of southeast China urban boundary layer air, are advected northeastward and upward ahead of the surface low.

Figure 3. UWNMS forecast for 0300 UT March 24, 2001 (11 am March 24 local time), showing sea level pressure (white contours, interval 4 hPa) and a vertical section with potential temperature (black contours, interval 10 K), the 0.1 m/s vertical velocity isosurface in pink, and the passive tracer initialized to be 1 at the surface (red) to 0 at 22 km (dark blue).

Figure 4. UWNMS forecast for 0400 UT March 24, 2001 (noon local time), showing a horizontal slice at 12.5 km altitude of ppmv ozone (color index) and potential vorticity (black contours, 1 PVU interval). The subtropical jet is shown by the 53 m/s isosurface.

Figure 5. Horizontal projection of DC8 TRACE-P flight 14 during 2330 UT March 23 - 0830 UT March 24, 2001 (8:30 am to 5:30 pm local time), superimposed on an infrared image from the GMS-5 satellite at 0332 UT (12:32 pm local time).

Wirth, V., and J. Egger, Diagnosing extratropical synoptic-scale stratosphere-troposphere exchange: A case study, *Q. J. R. Meteorol. Soc.*, **125**, 635-655, 1999.

Figure 6. Time-height section of Langley DIAL ozone mixing ratio in ppbv for flight 14. Note the break in time near 0600 UT when the plane was in the clouds.

Figure 7. Flight 14 a) altitude in km and b) ozone mixing ratio in ppbv.

Figure 8. Ozone in ppmv at flight level shown as vertical profiles for the periods a) 2328 UT March 23 - 0047 UT March 24, ascent from Yokota, b) 0158 - 0219 UT March 24, descent near 26°N, 150°E, c) 0246 - 0316 UT March 24, ascent near 26°N, 150°E for MOPITT underpass, d) 0410 - 0437 UT March 24, descent near 22°N, 142°E, e) 0616 - 0715 UT March 24, ascent in the convective complex near 28°N, 136°E, and f) 0740 - 0819 UT March 24, descent into Yokota.

Figure 9. UWNMS ozone hindcast at 30 km resolution for 0100 UT March 24, 2001 (10 am local time), contour interval 50 ppbv: a) horizontal section at 6.5 km and b) vertical section parallel to flight track, with a view toward the north.

Figure 10. As in Figure 9, except at for 0700 UT March 24, 2001 (4 pm local time) and a) horizontal section at 9 km and b) vertical section parallel to flight track, with a view toward the east.

Figure 11. UWNMS hindcast for 0400 UT March 24, 2001 (1 pm local time), showing 10 km streamlines, potential vorticity (black contours from 0.9 to 2.4 PVU, interval 0.3), and ozone flux (shading range $\pm 27 \times 10^{16}$ molecules $m^{-2}s^{-1}$).

Figure 12. As in Figure 11, except showing streamlines in a vertical section through the convective complex, with potential vorticity (black contours from 0.9 to 2.4 PVU, interval 0.3), and ozone flux. Note the ascent of boundary layer air to the upper troposphere in the convective complex and the downward ozone flux on the periphery.

Figure 13. Time variation of horizontally integrated ozone flux across the 1.3 PVU surface for the 30 km UWNMS hindcast during 0000 UT March 22 - 1200 UT March 24, 2001.

Figure 14. Time record for DC8 flight 14 during 2320 UT March 23 - 0815 UT March 24 of mixing ratio in pptv for a) methanol, b) ethanol, and c) butanol.

Figure 15. UWNMS hindcast of butanol mixing ratio (ppbv) at 10 km for 0800 UT March 24, 2001 (5 pm local time) with a) no removal mechanism and b) wet removal only.

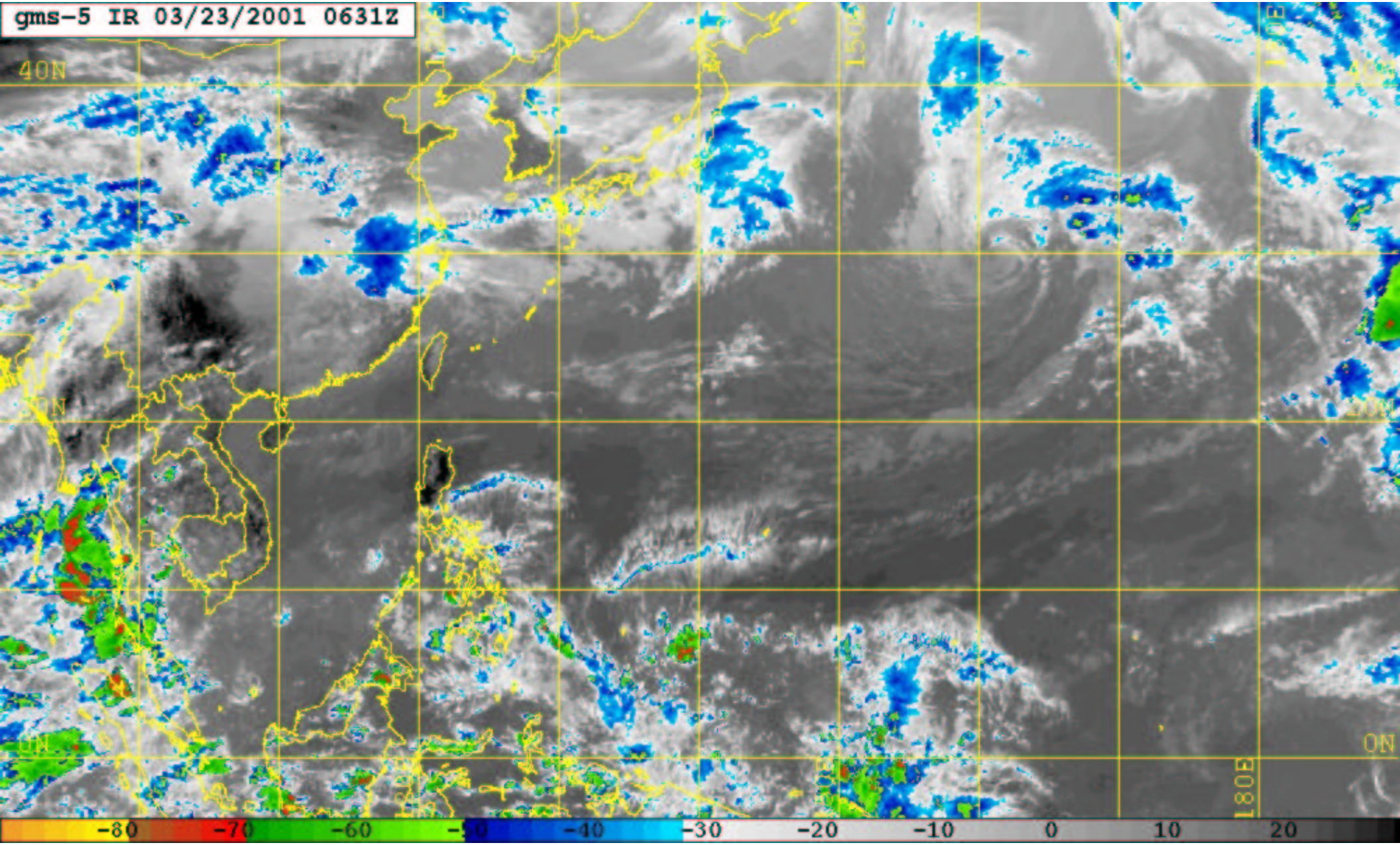
gms-5 IR 03/23/2001 0631Z
40N
150E
-80
-70
-60
-40
-30
-20
-10
0
10
20

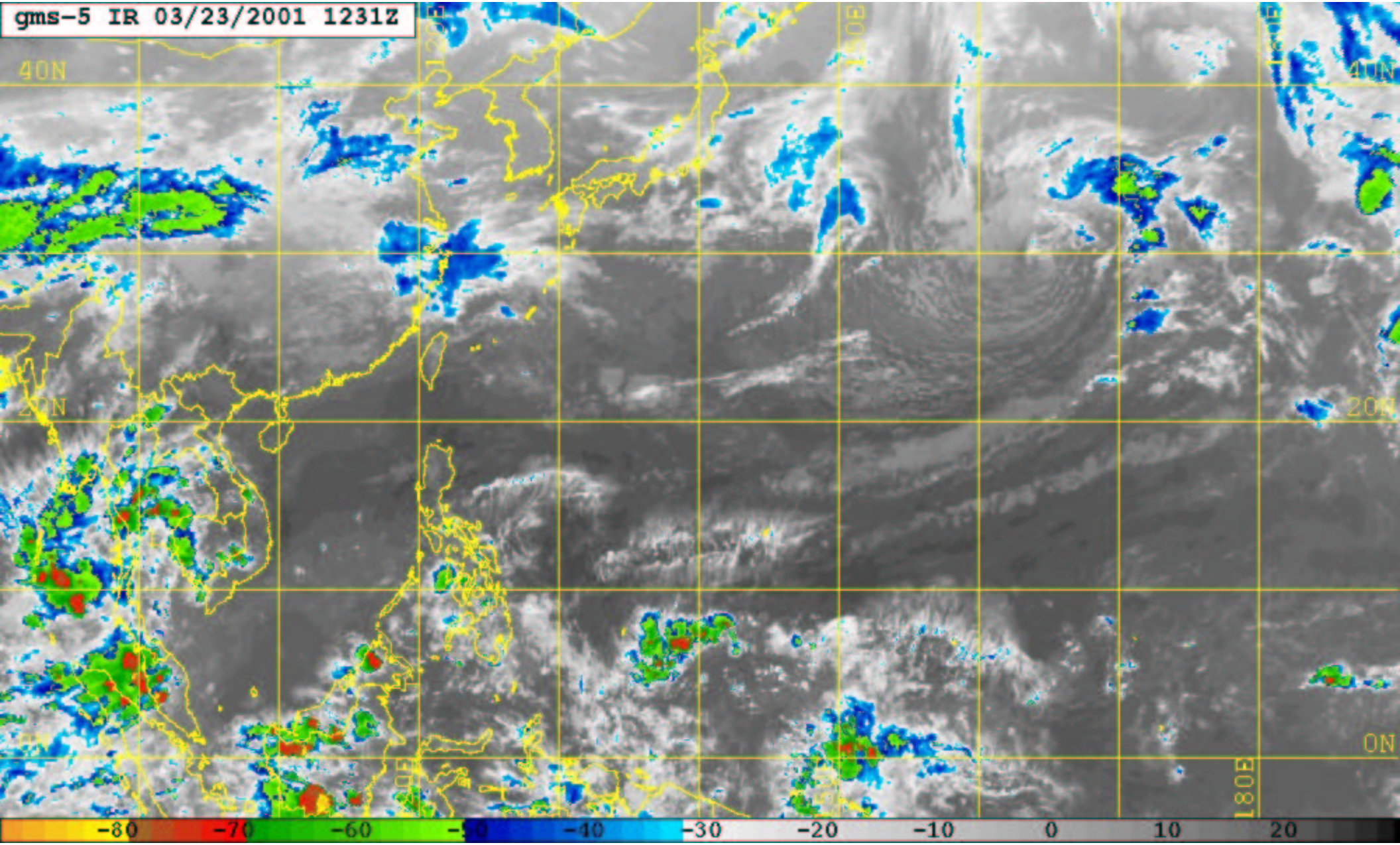
gms-5 IR 03/23/2001 1231Z
40N
20N
0N
120E
150E
180E
150E
180E
-80
-70
-60
-50
-40
-30
-20
-10
0
10
20

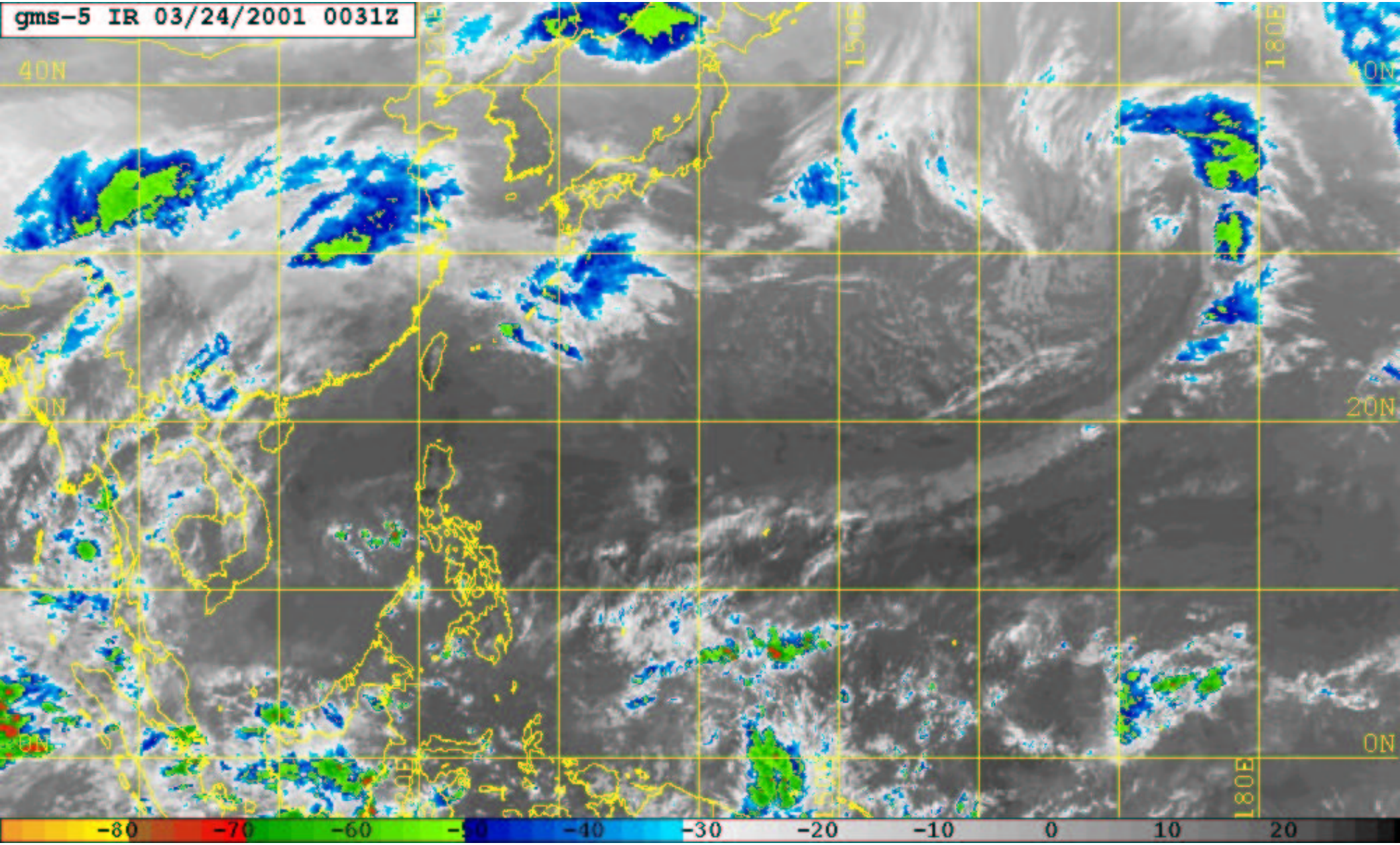
gms-5 IR 03/24/2001 0031Z
40N
20N
0N
120E
150E
180E
180E
-80
-70
-60
-50
-40
-30
-20
-10
0
10
20

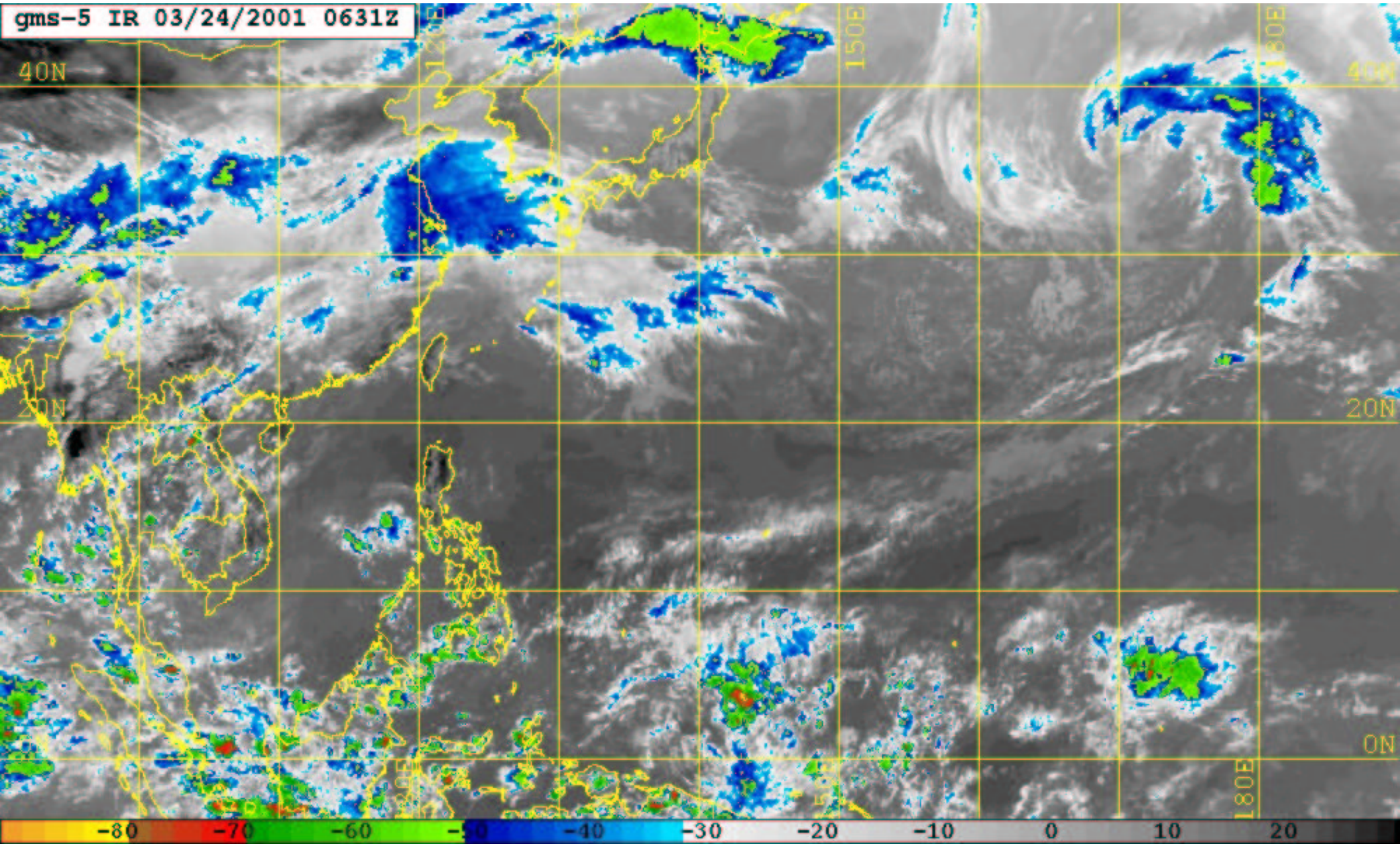
gms-5 IR 03/24/2001 0631Z
40N
20N
0N
150E
180E
-80
-70
-60
-50
-40
-30
-20
-10
0
10
20

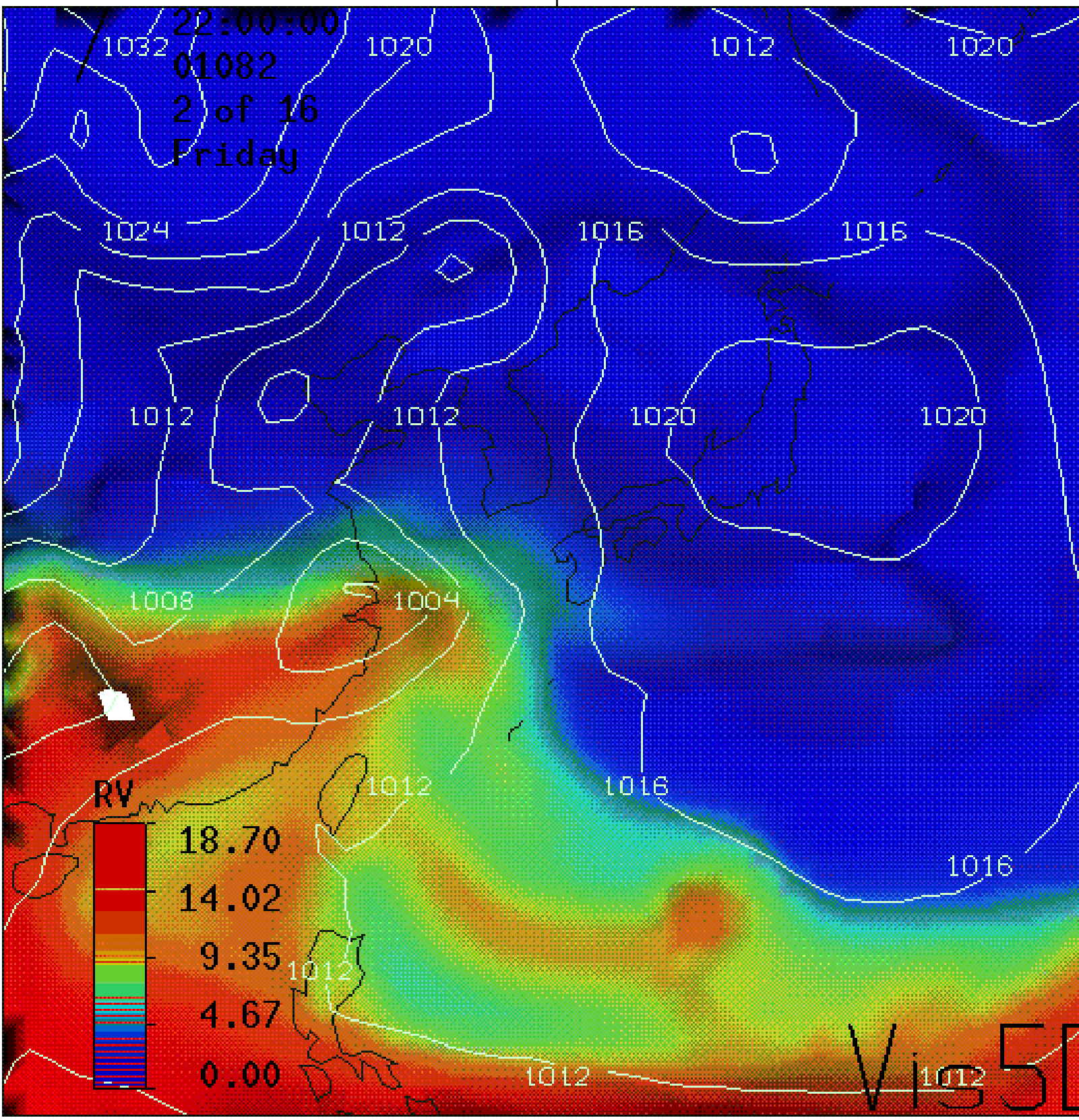
22:00:00
01082
2 of 16
Friday
1032
1020
1012
1020
1024
1012
1016
1016
1012
1012
1020
1020
1008
1004
RV
18.70
14.02
9.35
4.67
0.00
1012
1016
1016
1012
1012
Vis

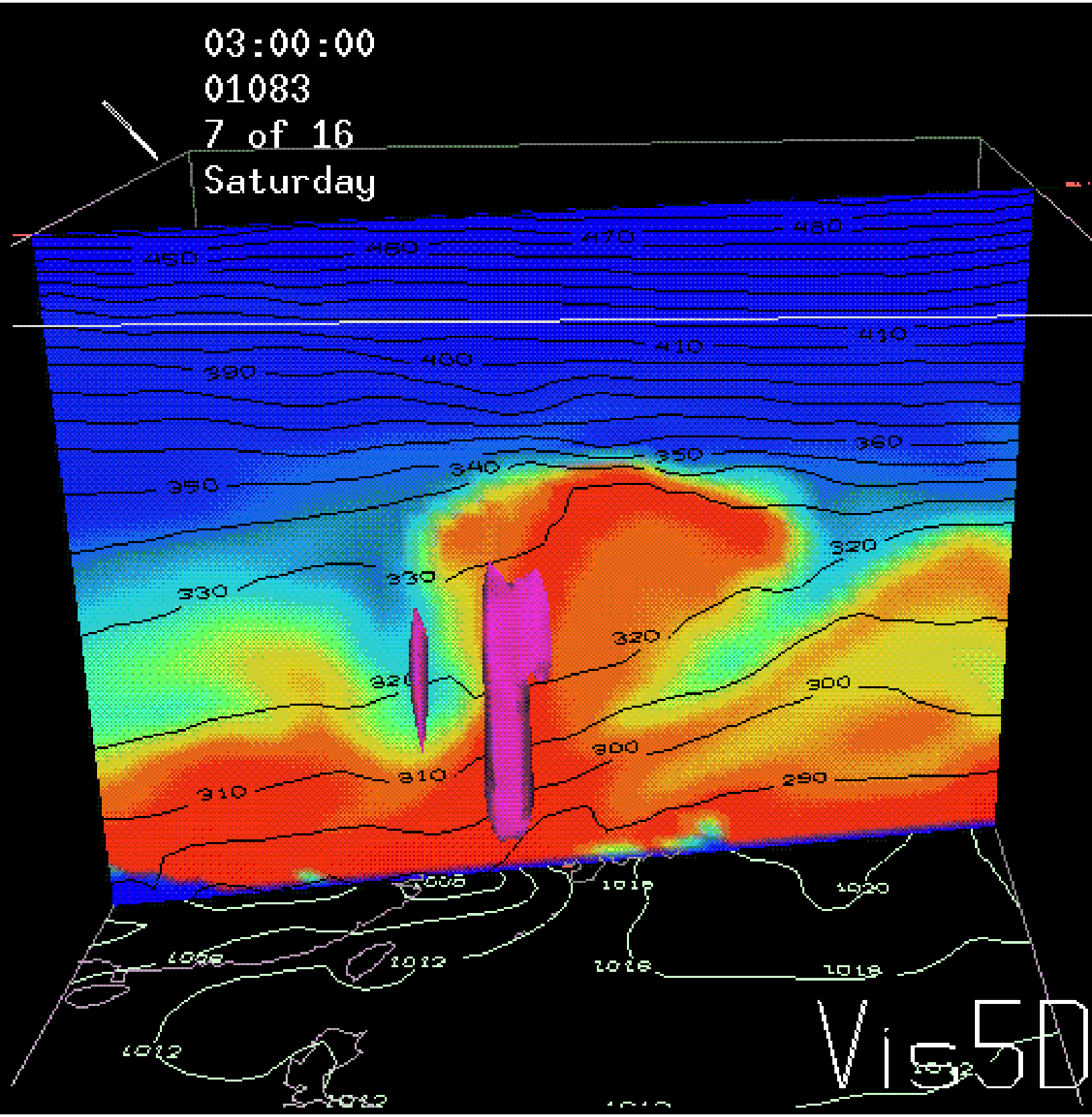
03:00:00
01083
7 of 16
Saturday
450
460
470
460
410
400
390
410
360
350
340
350
320
330
330
320
320
300
300
310
310
290
1008
1016
1020
1008
1012
1016
1018
1012
1012
Vis5D

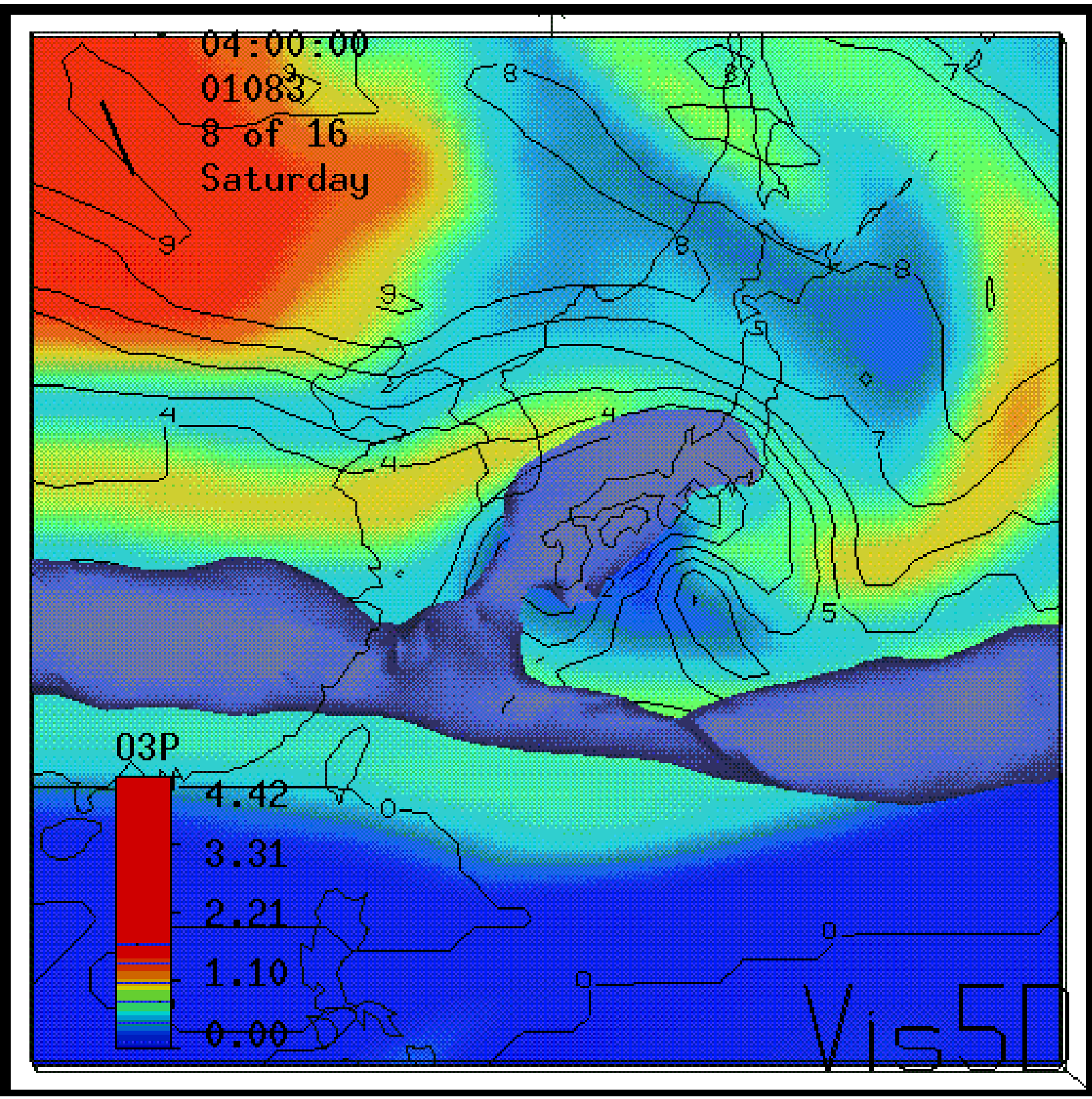
04:00:00
01083
8 of 16
Saturday
03P
4.42
3.31
2.21
1.10
0.00
VIS5D

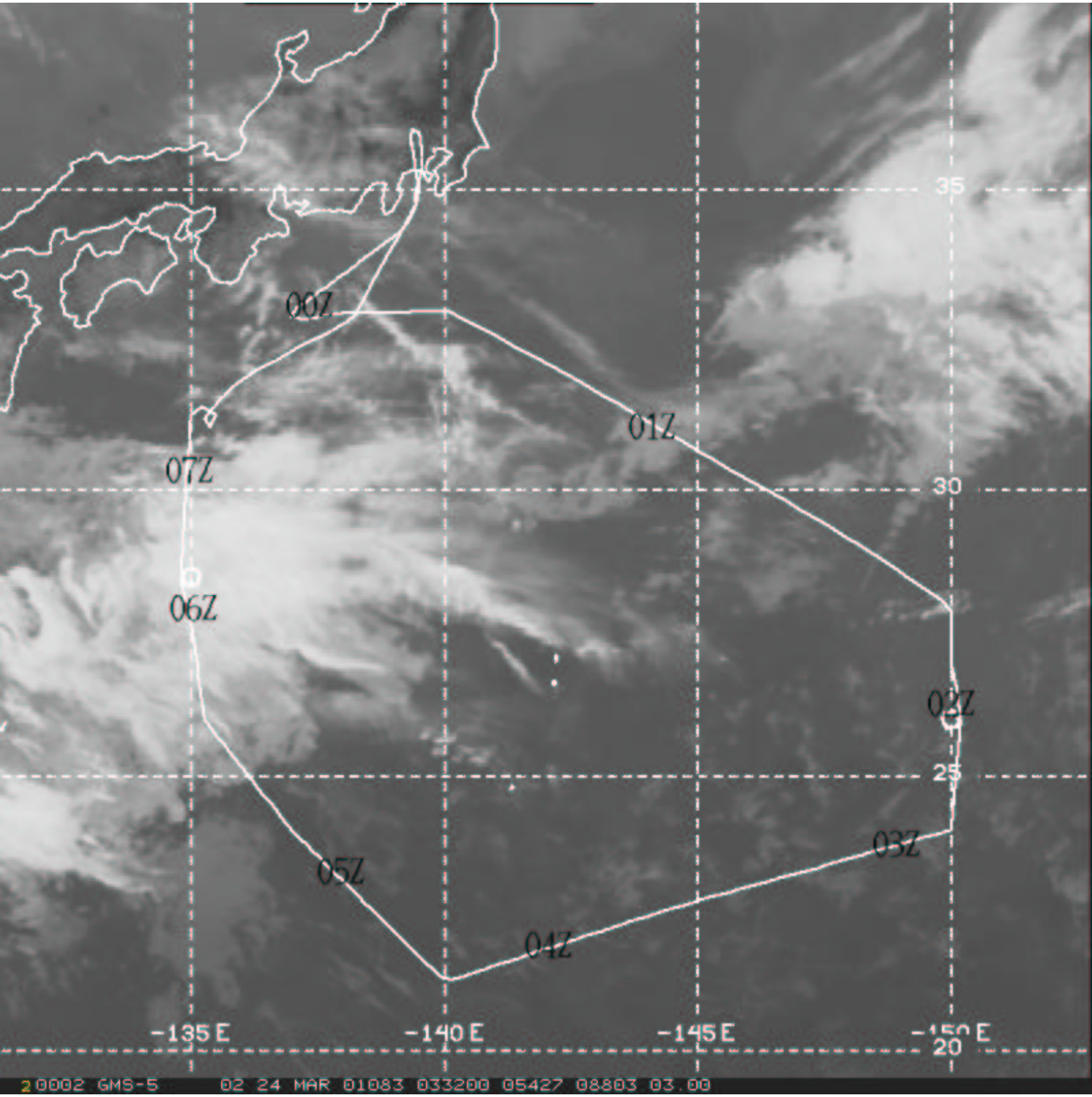
00Z
01Z
07Z
06Z
02Z
05Z
03Z
04Z
35
30
25
20
-135 E
-140 E
-145 E
-150 E
200002 GMS-5 02 24 MAR 01083 033200 05427 08803 03.00

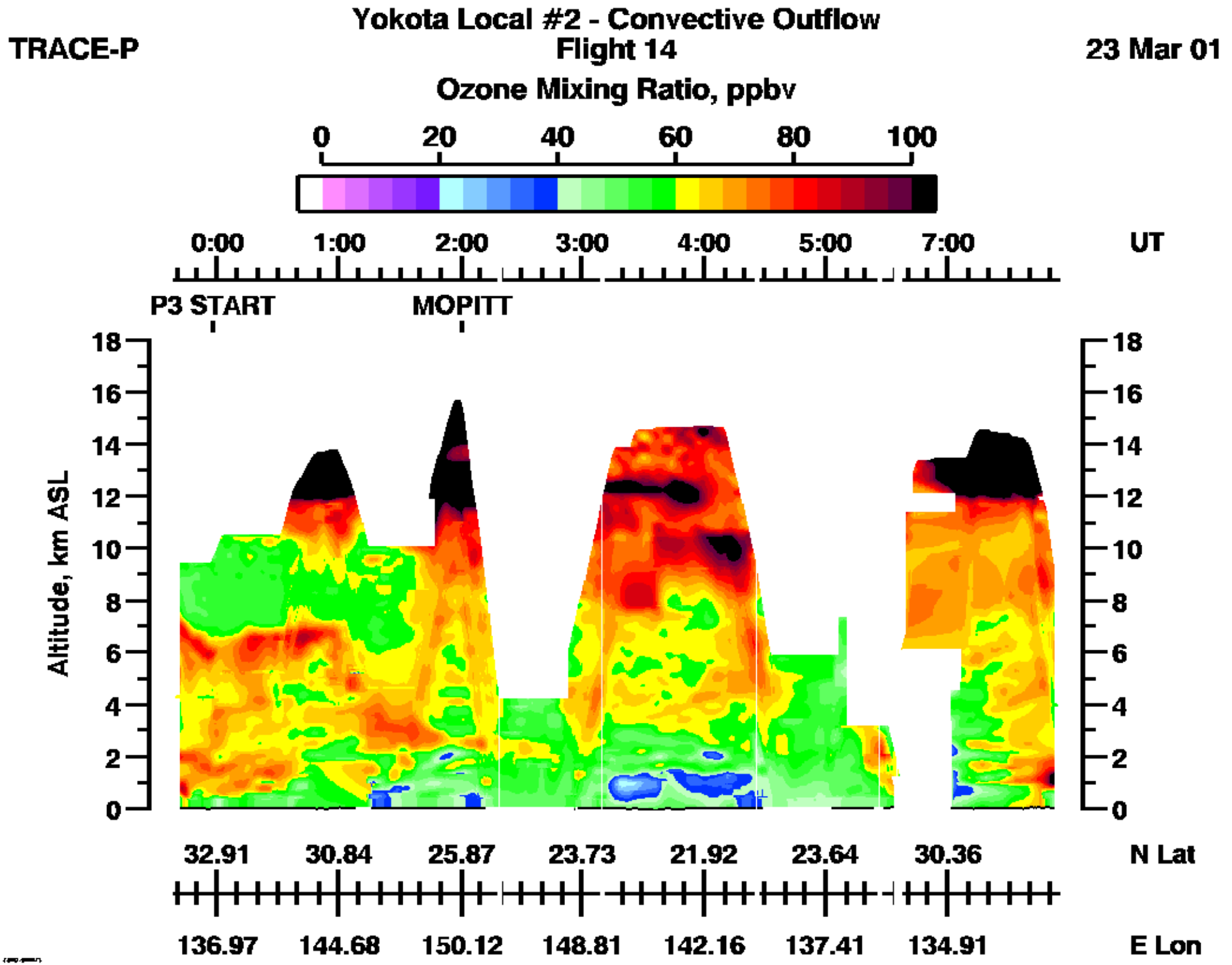
Yokota Local #2 - Convective Outflow
TRACE-P
Flight 14
23 Mar 01
Ozone Mixing Ratio, ppbv
0
20
40
60
80
100
0:00
1:00
2:00
3:00
4:00
5:00
7:00
UT
P3 START
MOPITT
Altitude, km ASL
18
16
14
12
10
8
6
4
2
0
32.91
30.84
25.87
23.73
21.92
23.64
30.36
N Lat
136.97
144.68
150.12
148.81
142.16
137.41
134.91
E Lon

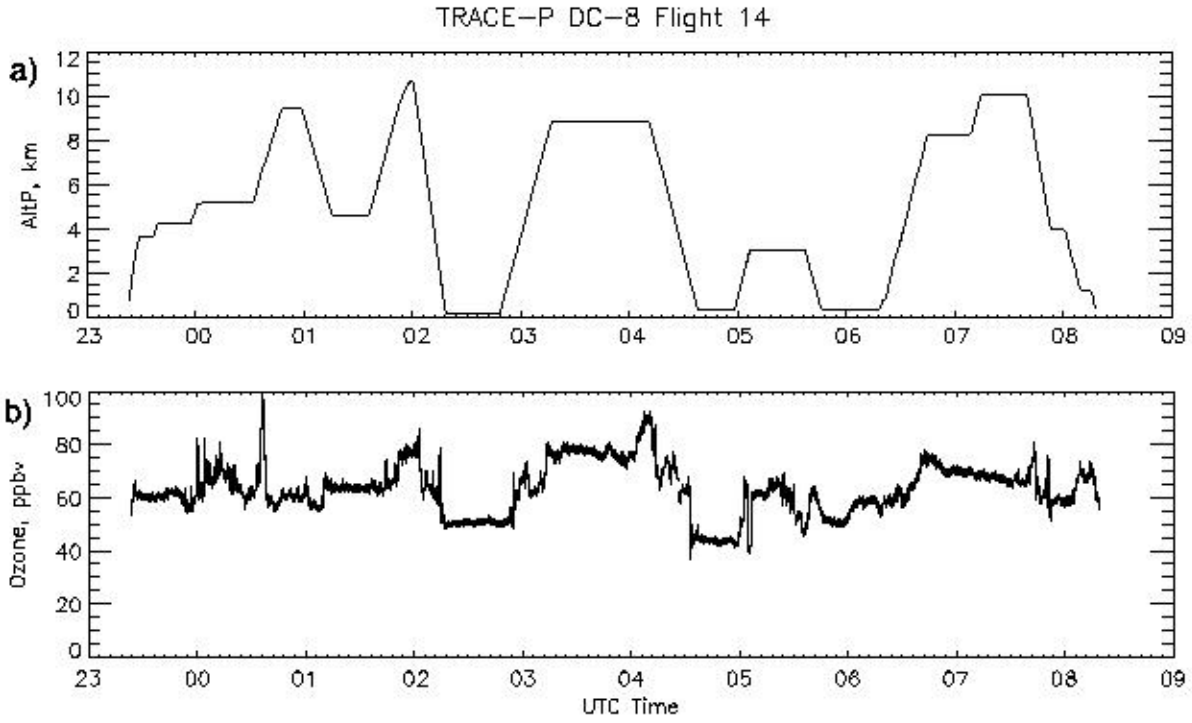
TRACE-P DC-8 Flight 14
a)
AltP, km
0
2
4
6
8
10
12
23
00
01
02
03
04
05
06
07
08
09
b)
Ozone, ppbv
0
20
40
60
80
100
UTC Time

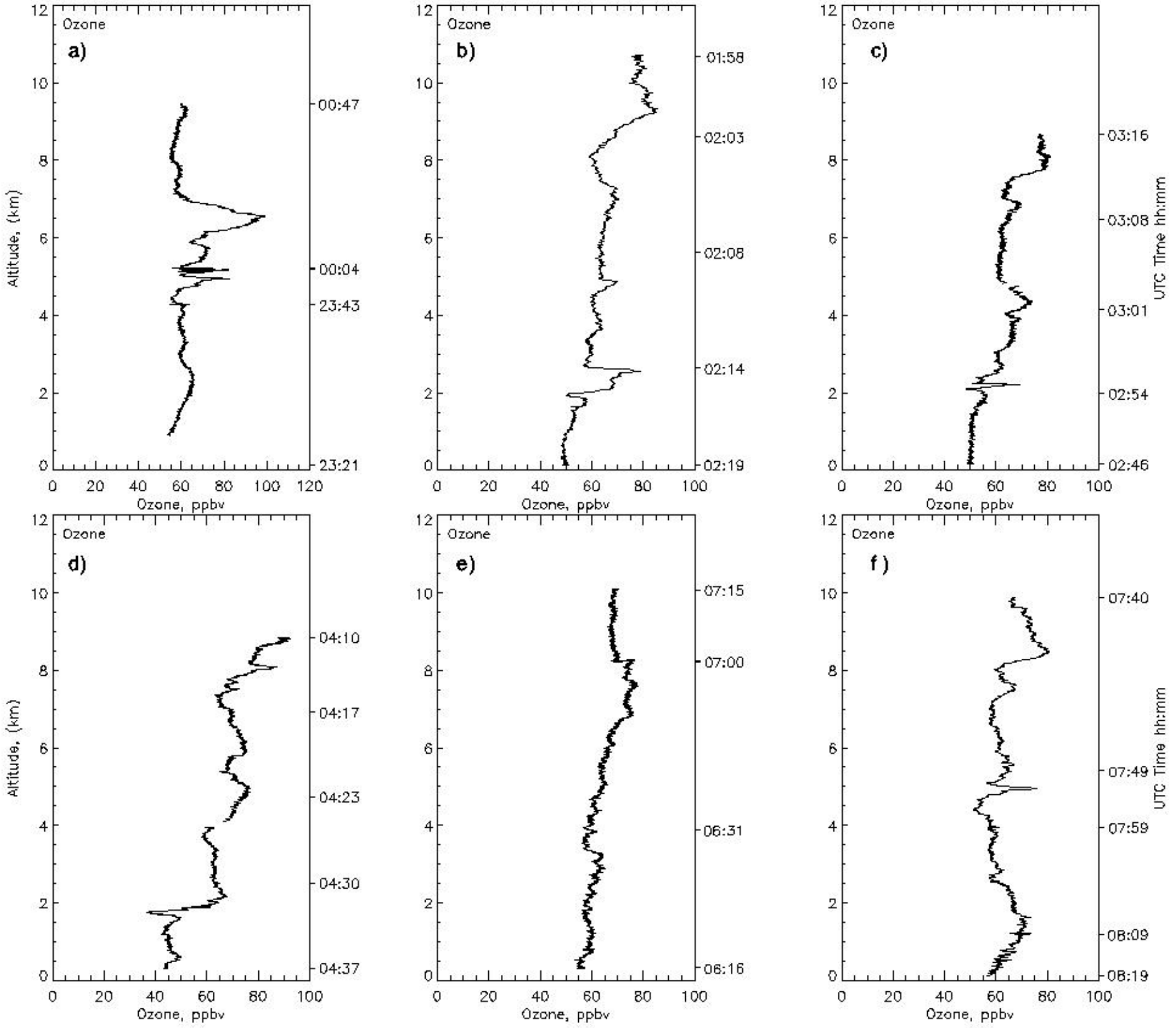
Ozone
a)
b)
c)
d)
e)
f)
Altitude, (km)
Ozone, ppbv
UTC Time hh:mm
00:47
00:04
23:43
23:21
01:58
02:03
02:08
02:14
02:19
03:16
03:08
03:01
02:54
02:46
04:10
04:17
04:23
04:30
04:37
07:15
07:00
06:31
06:16
07:40
07:49
07:59
08:09
08:19

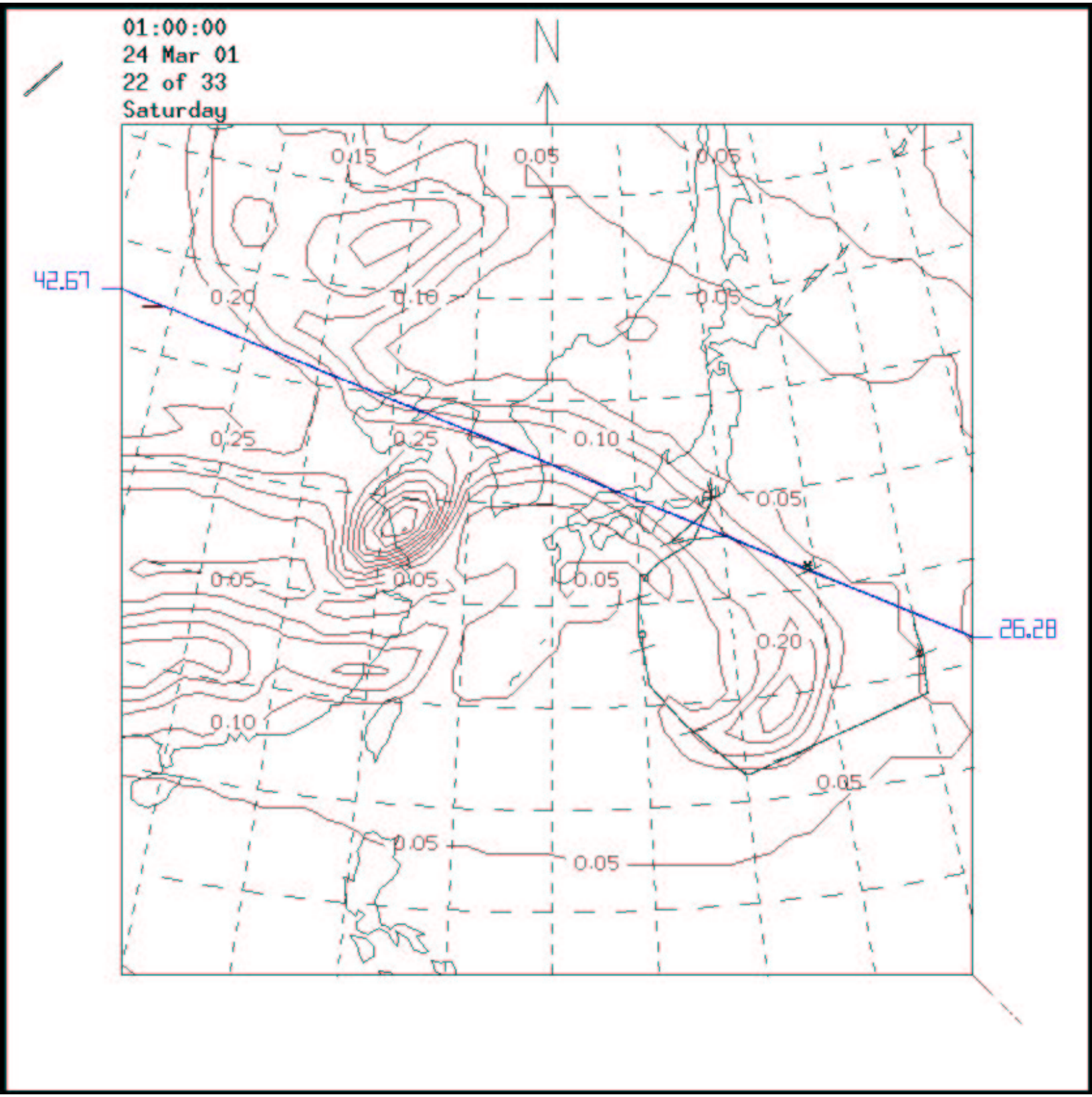
01:00:00
24 Mar 01
22 of 33
Saturday
N
42.67
26.28
0.15
0.05
0.05
0.20
0.10
0.05
0.25
0.25
0.10
0.05
0.05
0.05
0.05
0.20
0.10
0.05
0.05
0.05

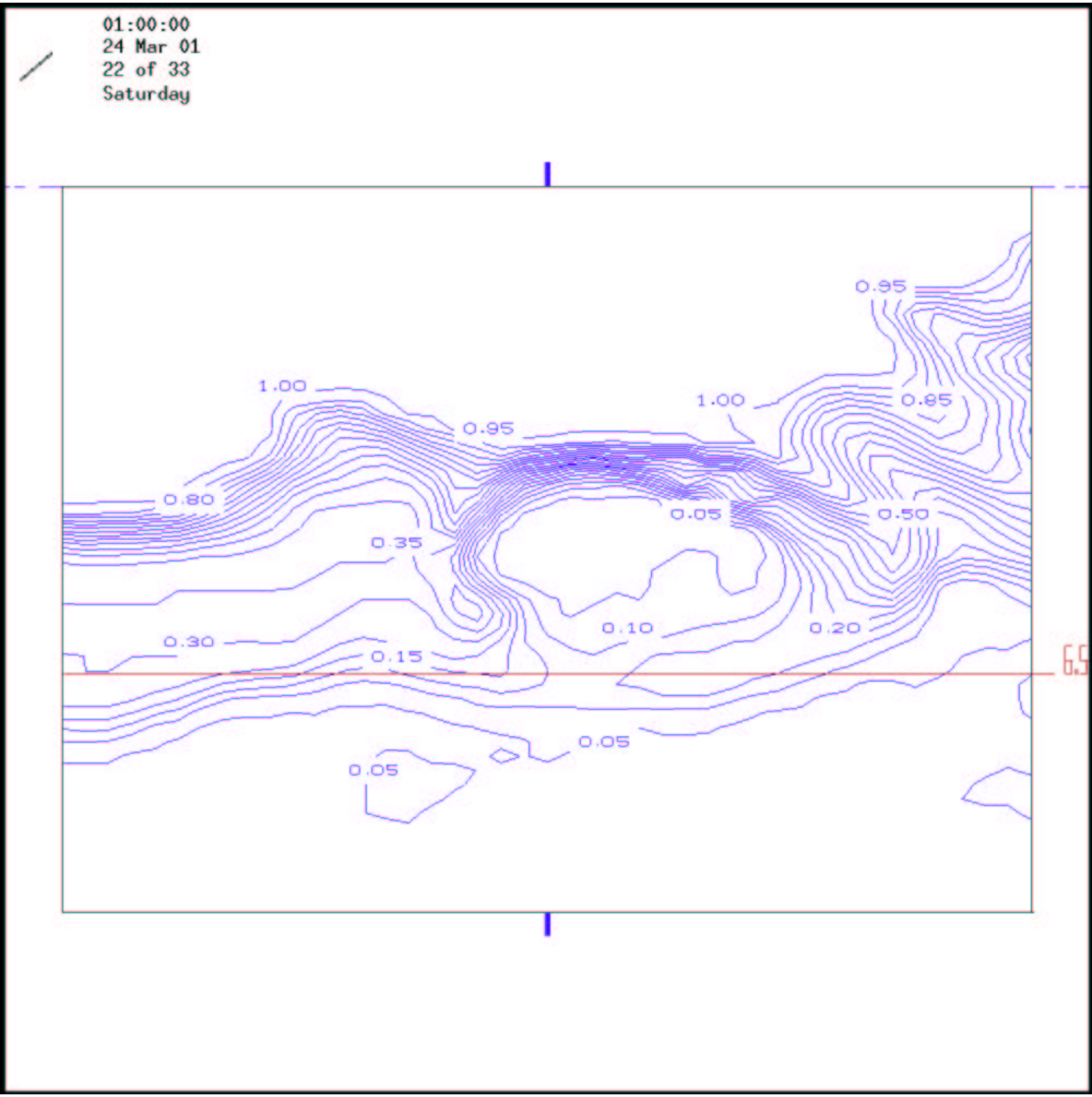
01:00:00
24 Mar 01
22 of 33
Saturday
0.95
1.00
0.85
1.00
0.95
0.80
0.05
0.50
0.35
0.10
0.20
0.30
0.15
0.05
0.05

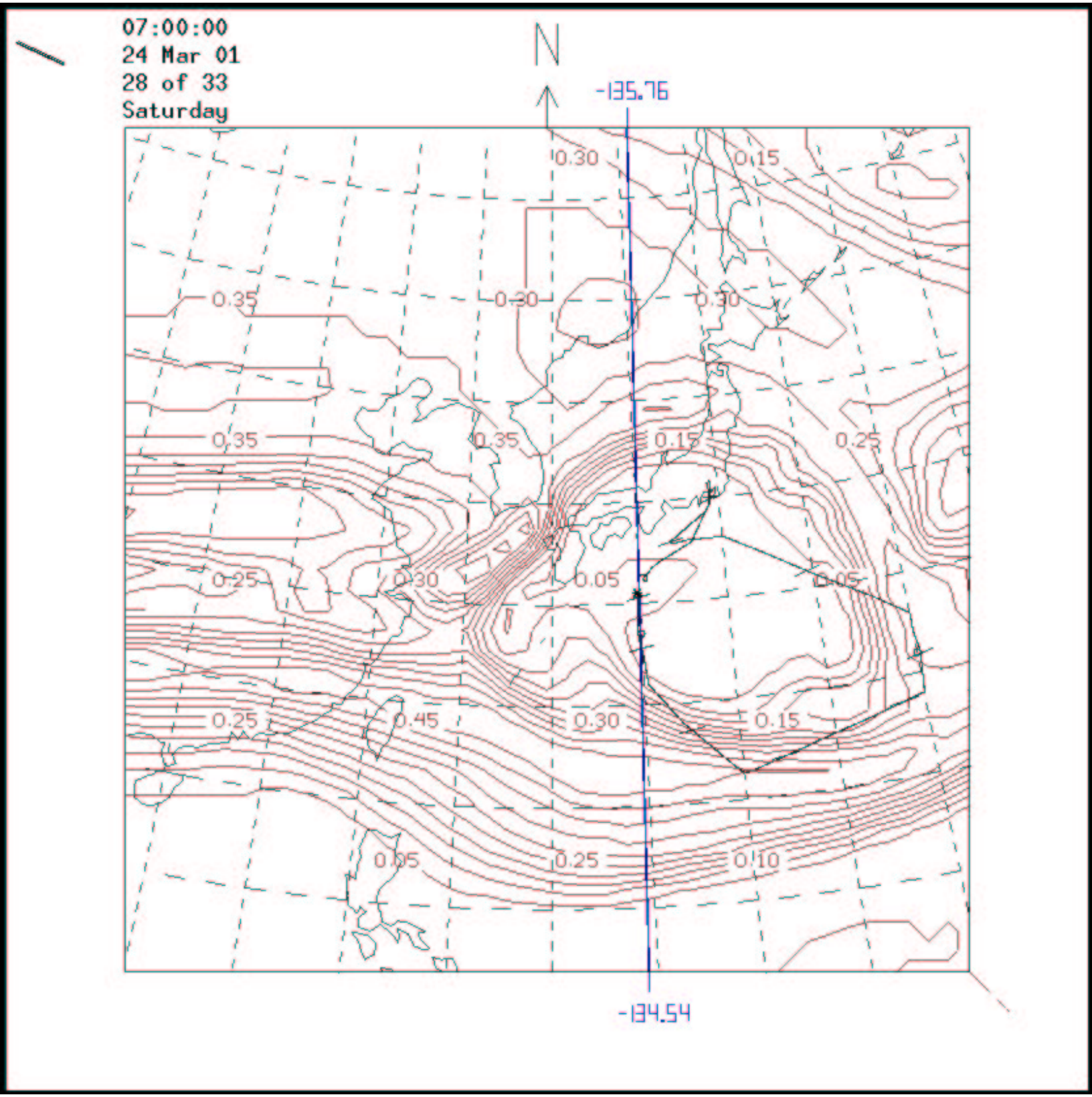
07:00:00
24 Mar 01
28 of 33
Saturday
N
-135.76
-134.54
0.30
0.15
0.35
0.30
0.30
0.35
0.35
0.15
0.25
0.25
0.30
0.05
0.05
0.25
0.45
0.30
0.15
0.05
0.25
0.10

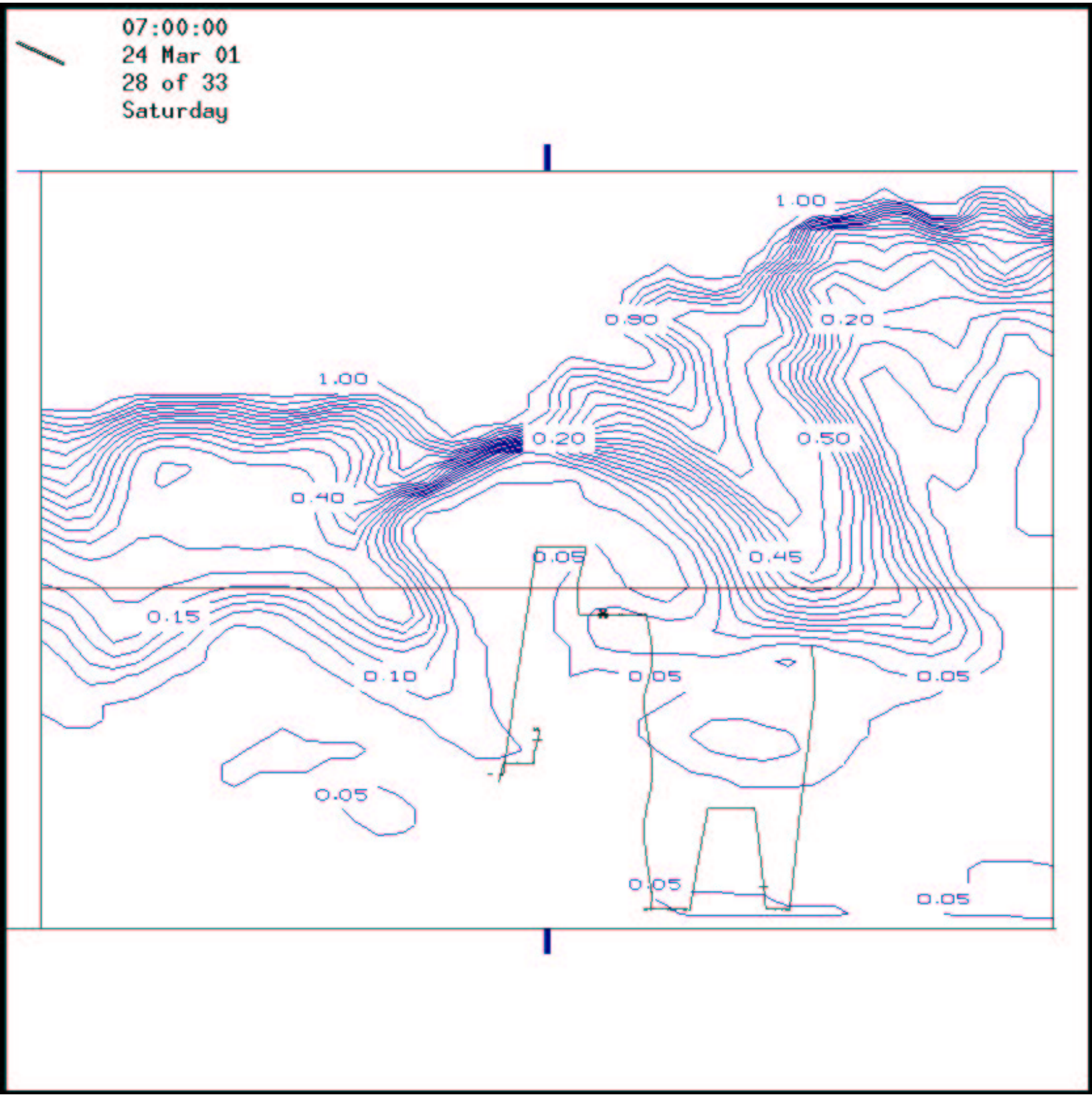
07:00:00
24 Mar 01
28 of 33
Saturday
1.00
0.90
0.20
1.00
0.20
0.50
0.40
0.05
0.45
0.15
0.10
0.05
0.05
0.05
0.05
0.05

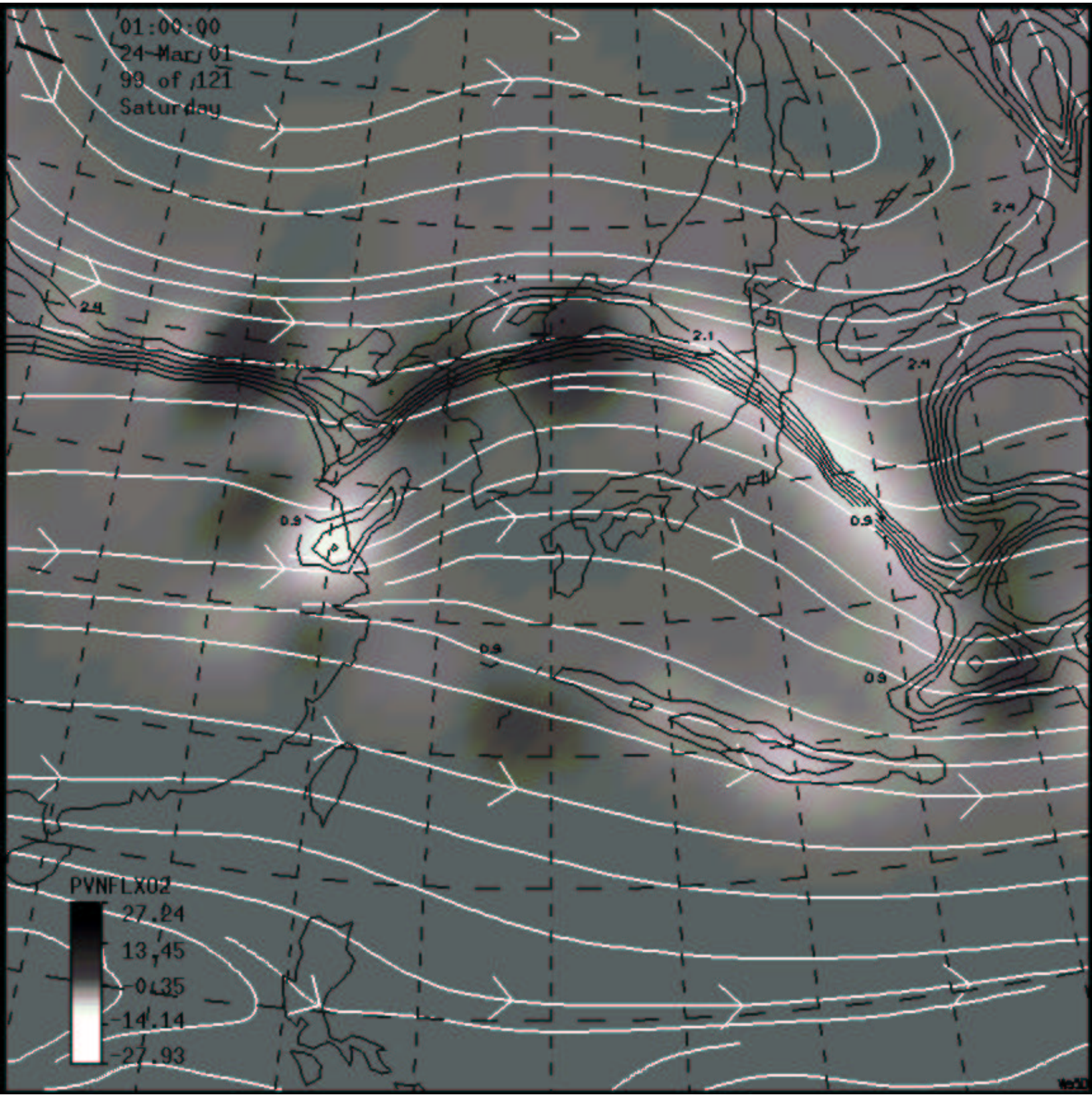
01:00:00
24-Mar-01
99 of 121
Saturday
2.4
2.4
2.1
2.4
0.9
0.9
0.9
0.9
PVNFLX02
27.24
13.45
-0.35
-14.14
-27.93

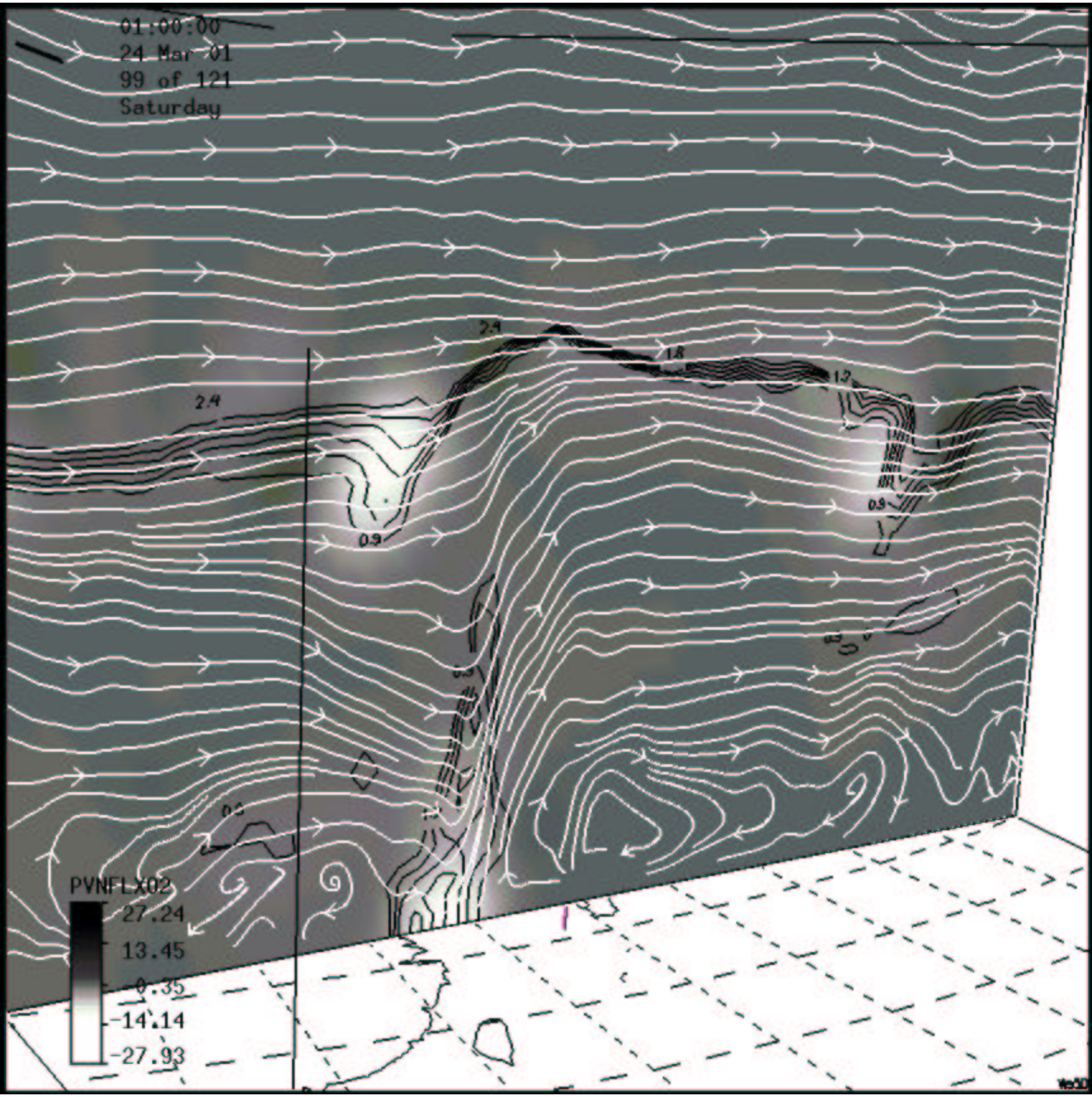
01:00:00
24 Mar 01
99 of 121
Saturday
2.4
1.8
1.2
2.4
0.9
0.9
PVNFLX02
27.24
13.45
-0.35
-14.14
-27.93

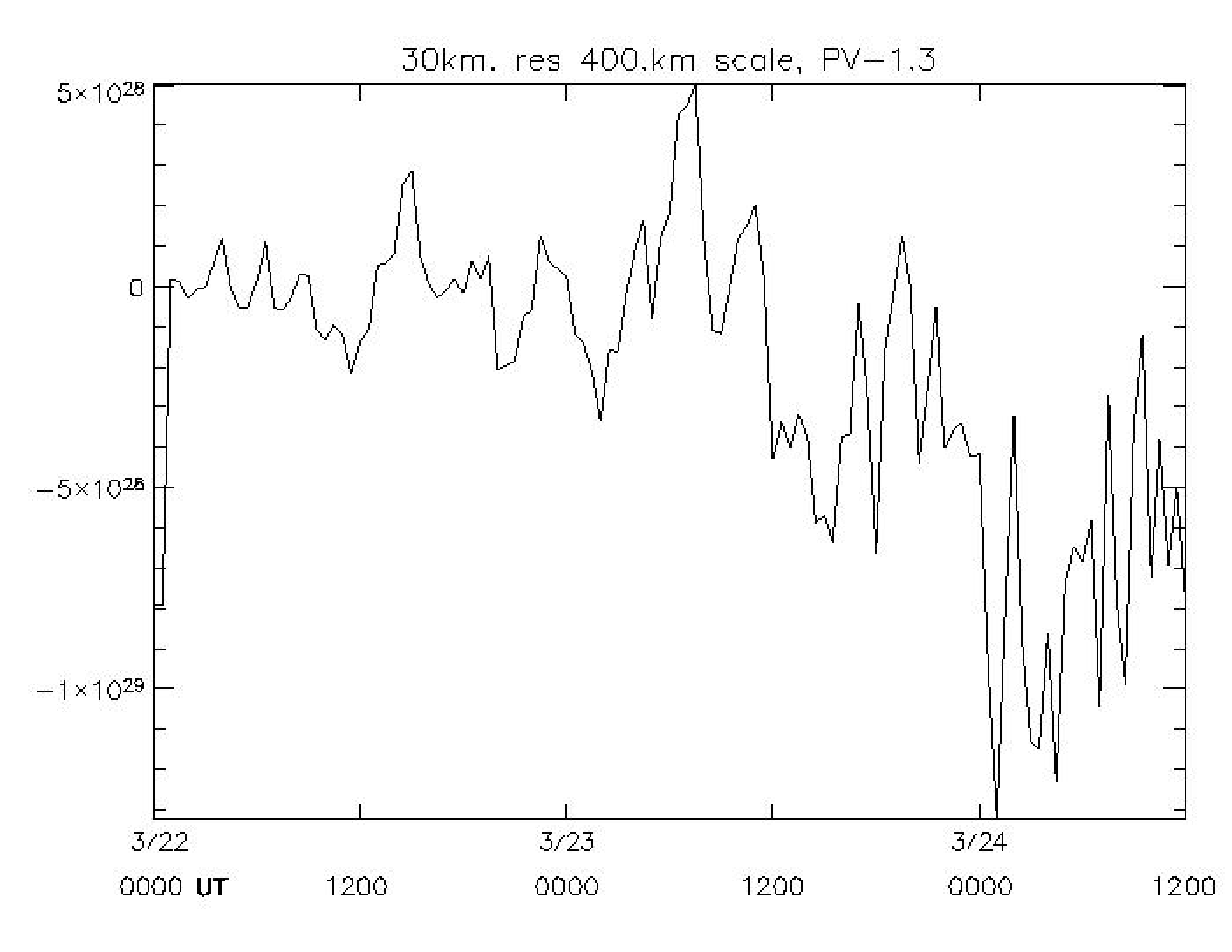
30km. res 400.km scale, PV−1.3
5×10²⁸
0
−5×10²⁸
−1×10²⁹
3/22
3/23
3/24
0000 UT
1200
0000
1200
0000
1200

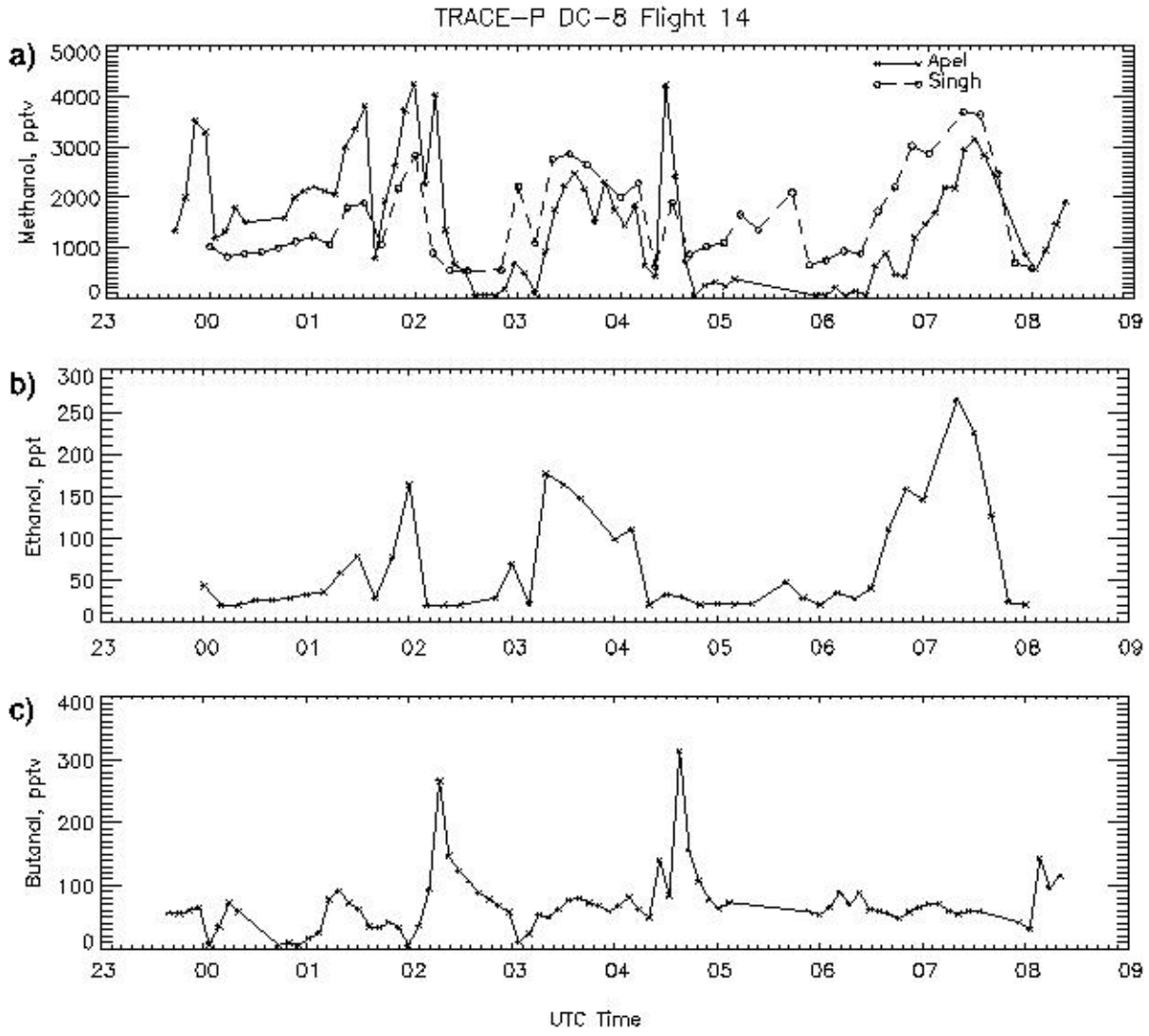
TRACE-P DC-8 Flight 14
a)
Methanol, pptv
5000
4000
3000
2000
1000
0
Apel
Singh
b)
Ethanol, ppt
300
250
200
150
100
50
0
c)
Butanal, pptv
400
300
200
100
0
23
00
01
02
03
04
05
06
07
08
09
UTC Time

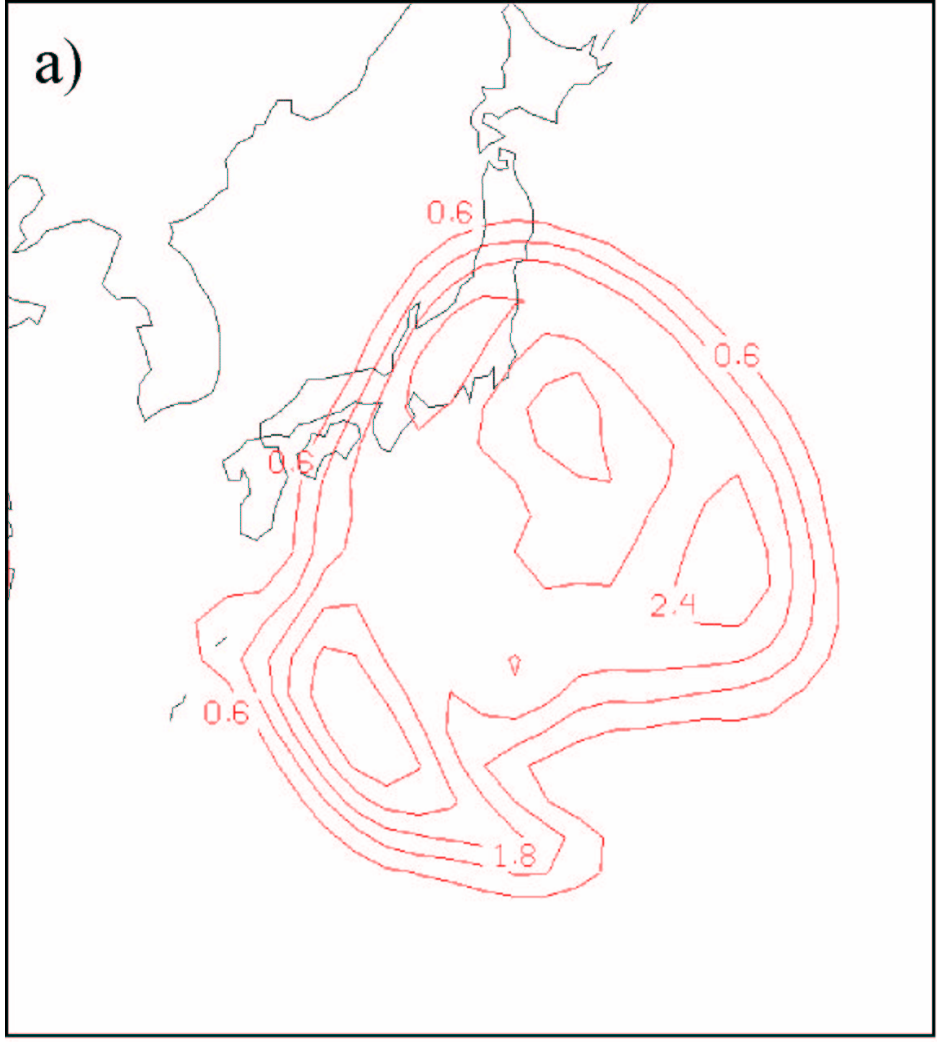
a)
0.6
0.6
0.6
2.4
0.6
1.8

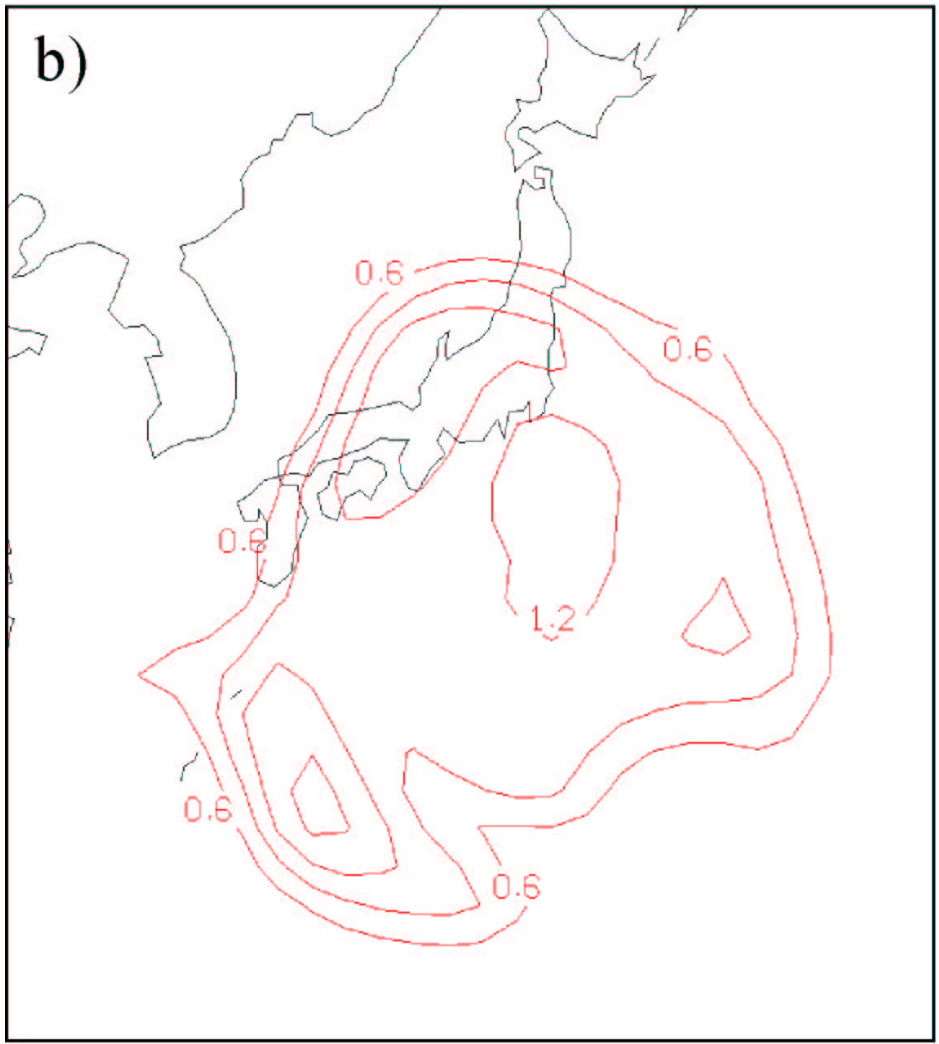
b)
0.6
0.6
0.6
1.2
0.6
0.6